Charge separation dynamics at bulk heterojunctions between poly(3-hexylthiophene) and PbS quantum dots

Yuliar Firdaus,[1] Rany Miranti,[2] Eduard Fron,[1] Adis Khetubol,[1] Erwin Vandenplas,[3] David Cheyns,[3] Holger Borchert,[2] Jürgen Parisi,[2] Mark Van der Auweraer [1,a)]

[1] *Laboratory of Photochemistry and Spectroscopy, Division of Molecular Imaging and Photonics, Chemistry Department, KULeuven, Celestijnenlaan 200F, B2404, 3001 Leuven, Belgium*

[2] *University of Oldenburg, Department of Physics, Energy and Semiconductor Research Laboratory, Carl-von-Ossietzky-Str. 9-11, 26129 Oldenburg, Germany*

[3] *Imec vzw, Kapeldreef 75, 3001 Leuven, Belgium*

Abstract

Photo-induced electron transfer between P3HT and small (2.4 nm) PbS QDs, capped by different ligands, was studied by picosecond and femtosecond time-resolved fluorescence and by photo-induced absorption (PIA) measurements. In line with previous experiments, we observed that the efficiency of the quenching of P3HT by PbS QDs increased upon decreasing the average thickness of the ligand shell. This trend was also observed in the PIA spectra and in prior work on the performance of photovoltaic devices where the active layer was a blend of P3HT with PbS QDs capped by different ligands. Combining the pico- and femtosecond fluorescence decays showed that the quenching in blend films of P3HT and PbS QDs treated with 1,4-benzenedithiol occurred over a broad time scale ranging from tens of femtoseconds to hundreds of picoseconds. This complex kinetics was attributed to exciton hopping followed by electron transfer to the conduction band of the QDs. We also compared the wavelength dependence of the internal quantum efficiency (IQE) in the hybrid photovoltaic devices to those devices where the photoactive layer consists of PbS QDs only. While excitation in the first excitonic transition of the PbS QDs yielded a similar IQE in both devices, the IQE of the hybrid devices tripled at wavelengths where also P3HT started to absorb. This suggests that upon excitation of P3HT in the latter devices charge generation occurs by photo-induced electron transfer from P3HT to the QDs rather than by energy transfer to the QDs followed by exciton dissociation in the QDs.

[a)] Author to whom correspondence should be addressed. Electronic mail: mark.vanderauweraer@chem.kuleuven.be.

I. INTRODUCTION

For the past several decades, intensive research has been underway to develop low-temperature and solution processed photovoltaic devices (PVs) through the use of nanostructured materials such as colloidal inorganic quantum dots (QDs)[1,2] and conjugated polymers.[3,4] Using lead chalcogenide (e.g. PbS, PbSe) QDs with a near-infrared band-gap, the power conversion efficiency (PCE) of purely QD based photovoltaic devices (PVs) has increased to values over 8%.[5,6] Meanwhile, organic photovoltaic devices (OPVs) with a PCE exceeding 10% have been demonstrated.[7] Hybrid bulk heterojunctions between inorganic QDs and conjugated polymers are of significant interest[8–11] as they have the potential to combine the advantages of both material classes as *e.g.* the large molar extinction coefficient of the conjugated polymers, the band gap tunability and (photo)stability of the QDs and the potential for multiple exciton generation (MEG) of the QDs[12]. However, their performance is still behind that of both purely inorganic and purely organic devices. Early bulk heterojunction hybrid devices made with PbSe or PbS QDs and traditional conjugated polymers such as poly-thiophenes or poly-p-phenylene-vinylene derivatives yielded a low PCE ranging from 0.0013% to 0.7%,[13–16] which has been attributed to inefficient photo-induced charge transfer related to the formation of poor type-II heterojunctions.[17] The combination of PbS QDs with conjugated polymers with a high-lying highest occupied molecular orbital (HOMO) and a better PbS surface passivation led to a dramatic increase of the PCE of hybrid PVs which then attained values from 0.55% to 4.23%.[8–10,18,19] The state of the art for hybrid PVs is represented by the blend of PbS_xSe_{1-x} QDs and a conjugated polymer with a high-lying HOMO yielding a PCE of 5.5%.[20]

These new polymers have been reported to support long-lived (microsecond and longer) photo-induced charge separation at the polymer:PbS interface leading to a consequent increase of the photocurrent.[21,22] However, we recently showed that the use of small (2.4 nm) PbS QDs and post-deposition ligand exchange to 1,4-benzenedithiol (BDT) improves the PCE of photovoltaic devices based on poly-(3-hexylthiophene) (P3HT) and PbS QDs up to almost 1% using a simple bulk heterojunction device architecture.[11] The improvement was attributed to the formation of an energetically favorable type II heterojunction between P3HT and PbS QDs when small size (2.4 nm) PbS QDs were used and to the use of more suitable ligands. [11] Generally, in hybrid photovoltaic devices, light absorption by the conjugated polymer or QDs creates excitons that dissociate into free charges by electron (hole) transfer at the boundary of both materials. Direct evidence for both processes (electron or hole transfer) has been obtained in a number of polymer:QDs blend systems.[8,21,22] However, other pathways for photocurrent generation exist. Photocurrents could also arise due to light absorption by the polymer followed by energy transfer to the QDs and hole transfer.[21] Light absorption by the QDs could also directly lead to exciton dissociation in the QDs due to band bending and the resulting electric field near the contacts. [23,24] The latter phenomenon has been known to

produce large photocurrents even in the absence of any polymer in Schottky type PVs where the Schottky barrier is situated at the contact between the QD layer and the (metal) cathode.[6,25-28]

Therefore, in this paper we investigated the charge separation and related it to the device performance in hybrid photovoltaic devices using P3HT as hole transport polymer and small size PbS QDs as electron acceptor. Photoluminescence (PL) quenching and photo-induced absorption (PIA) measurements were carried out on samples prepared under experimental conditions similar to the photovoltaic devices in order to provide insight into the kinetics of the charge separation. We also showed that the device performance of photovoltaic devices based on neat PbS QDs and blended P3HT:PbS films can be further increased by device optimization. Taking into account that in the best performing device[11] the volume fraction of P3HT was only 19% (see table S1[29]) we also investigated a device with neat PbS-BDT QDs to find out if the hole transport polymer was necessary at all. The wavelength dependence of the internal quantum yield of this device also helped us to discriminate between quenching of the P3HT emission by energy and by electron transfer. The combination of the spectroscopic and photovoltaic device measurements provided us the opportunity to draw conclusions on several aspects of the P3HT:PbS hybrid system and to make a direct comparison between photovoltaic devices with hybrid blends and devices with an active layer consisting of only nanoparticles, respectively.

II. EXPERIMENTAL

A. Materials.

The colloidal PbS QDs with a core diameter of approximately 2.4 nm and capped by oleic acid (OLA) were purchased from Evident Technologies (Troy, NY). P3HT was obtained from Rieke Metals under the commercial name Sepiolid P200 (M_n=13.9 kg/mol, PDI=1.71, regioregularity>96%). All solvents used, *i.e.* acetonitrile, isopropyl alcohol, methanol, toluene, chloroform, chlorobenzene, were of spectroscopic grade. They were purchased from Sigma Aldrich and used as received.

B. Preparation of P3HT and P3HT:PbS blend films for Spectroscopy Experiments.

Quartz glass substrates were pre-cleaned in an ultrasonic bath with Hellmanex detergent, deionized water, acetone and isopropyl alcohol, and treated in an ultraviolet-ozone chamber for 30 minutes. Film samples were prepared by spin coating (1000 rpm, 60 s) a P3HT or a P3HT:PbS blend solution in chloroform on a clean quartz glass (sapphire substrate for PIA measurements) in a nitrogen filled glove box. The blend of P3HT:PbS QDs (60, 75, 90% loading of QDs, the loading corresponding to the ratio of the weight of the PbS QDs assuming no ligand shells to the sum of the weight of the PbS core and of P3HT) was dissolved in chloroform at a total concentration of about 20-38 mg/ml (considering the weight of PbS and that of P3HT), which is close to the concentration used for making the photovoltaic devices.[11] Starting from the composition

of the blend films it was in this way possible to estimate the weight and volume percent of the inorganic PbS QDs and of the ligands in the films taking into account the ligands using the procedure described in the Supporting Information (SI, Table S1[29]). The solutions were stirred for ~1 hour at 70°C. After spin-coating the films were annealed at 150°C for 10 minutes under nitrogen in a nitrogen filled glovebox. Except for the PIA measurement, the samples were encapsulated inside the glovebox in order to minimize the contact between the samples and air during measurements and to avoid oxidation or adsorption of oxygen, using the following procedure: the edge of the samples was cleaned by chloroform and then covered by epoxy glue and consecutively a clean quartz plate was pressed to the sample. The sample encapsulation is important because even when the fluorescence decay experiments were conducted in an evacuated sample compartment the non-encapsulated sample showed the occurrence of a photodegradation compared to the encapsulated ones. This can be due to incorporation of oxygen in the sample during the transport or incomplete oxygen removal from the vacuum chamber (pressure about 10^{-6} torr).

The PbS QDs discussed in this work were subjected to different routes of ligand exchange, namely post-deposition and solution-phase ligand exchange. The 1,4-benzenedithiol (BDT) ligand was used in post-deposition ligand exchange while octylamine (OAm) and octanethiol (OT) were used in solution phase ligand exchange. These ligand exchange processes are described in detail in Ref.10 and 11.

C. Steady State Spectroscopy.

Absorption spectra were measured with a Perkin Elmer Lambda 40 UV-Vis spectrophotometer. Fluorescence spectra were measured by excitation at 488 nm with a Fluorolog-3 FL3-22 Horiba Yobin Yvon spectrometer, which was corrected for the wavelength dependence of the throughput of the emission monochromator and the sensitivity of the detector.

D. Characterization of P3HT:PbS active layers.

The morphology of the active layers of the photovoltaic devices was determined with a Zeiss EM 902A transmission electron microscope (TEM). The films for the TEM measurements were formed by spin coating of the blend solutions (total concentration 7.6-12 mg/ml) onto a glass substrate covered by PEDOT:PSS. The spin-coated films were rinsed with water to lift-off the films from the glass substrate, and were then transferred to pure copper grids for the TEM experiments.

E. Picosecond Time-resolved Fluorescence Spectroscopy.

The fluorescence decays of the neat P3HT film and the P3HT:PbS blends were determined in the nanosecond – picosecond (ps) time range using time-correlated single photon counting (TCSPC). The TCSPC setup consists of a Tsunami Ti:Sapphire (Spectra Physics) laser pumped by a Millenia XS CW-laser (Spectra Physics), resulting in pulses of 2 ps which are tuneable between 760 and 1100 nm. The repetition rate was reduced to 8.1 MHz using a pulse picker (GWU).[30] The

frequen cy of the light is doubled with a flexible harmonic generator (GWU-FHG from GWU Lasertechnik). The power of the laser excitation (2 mm diameter) could be varied between 0.09 and 0.85 mW (corresponding to 0.01 to 0.1 nJ/pulse). The emission from the sample was detected at the magic angle (54.7°) polarization with a cooled R3809U-51 MCP-PMT (Hamamatsu) after passing through a subtractive monochromator. The resulting signals were processed using a SPC 430 (Becker & Hickl GmbH) computer card. The instrument response function (IRF) was recorded using a LUDOX scattering solution, and amounted to 20-30 ps (Full Width at Half Maximum (FWHM)). The fluorescence decay curves were analyzed by fitting the data to a convolution of the IRF with a decay function for a δ-pulse. The fitting is managed using a TRFA Global Analysis Program based on a Gaussian-weighted nonlinear least-square fitting with a Marquardt-Levenberg minimalization algorithm.[31,32] The quality of each fit was assessed by the random distribution of the residuals, their autocorrelation function and the value of the reduced chi-square parameter (χ^2), which was around 1.1.[31] All decays were fitted to the function: $I_{PL}(t) = \sum A_n exp\left(-\frac{t}{\tau_n}\right)$, where A_n and τ_n are fitting parameters. The average decay time was determined as $\langle\tau\rangle = \frac{\sum_i A_i\tau_i}{\sum_i A_i}$ (Eq.1). P_i, the contribution of each component to the stationary emission at the detection wavelength, is then given by $P_i = \frac{A_i\tau_i}{\sum_i A_i\tau_i}$.

F. Femtosecond Fluorescence Up-conversion (FFU) Spectroscopy.

The fluorescence decay in the ps - fs time-range was determined with fluorescence upconversion (FFU). An amplified femtosecond double OPA laser system was used to generate the excitation and gate pulses.[33] A mode locked Ti-Sapphire oscillator (Mai Tai SP, Spectra-Physics) was used to seed an amplifier comprising a pulse stretcher, a Ti-Sapphire regenerative cavity amplifier and a pulse compressor (Spitfire Pro 35F-XP, Spectra-Physics) which acts as the source of <35 fs pulses (FWHM), (31-nm bandwidth (FWHM), pulse energy 4 mJ) in the 800 nm range with a repetition rate of 1 kHz. The regenerative amplifier is energized by a Q-switched, diode-pumped Nd:YLF pulsed laser (Empower-30, Spectra-Physics) capable of delivering a 527 nm output beam of 30 Watts. The output of the amplifier is used to pump two identical two-stage optical parametric amplifiers (Topas-C, Light Conversion), each with 1 mJ pulse energy, in order to produce two excitation pulses (of which only one, tuned to 488 nm, is used in the present experiment), which are tunable independently between 300 and 2600 nm, with a duration of 60 fs (FWHM). Their bandwidth is 31 nm @ 500 nm (FWHM), and their energy amounts to about 100 μJ. After attenuation and focusing the sample is excited with pulses with an energy of 0.2 μJ and a diameter of 0.1 mm. Less than 1 percent of the output of the 800 nm amplifier (about 100 μJ) is used to produce gate pulses which are routed towards a mixing crystal (*cfr. infra*) via a computer controlled translation stage which generates a relative delay between excitation and gate pulses. The fluorescence light emitted from the sample (λ_{ex}=488 nm) was efficiently collected using a

concave mirror (Cassegrain), filtered for the scattered light, and directed into an LBO mixing crystal where it was overlapped with the gate pulse (800 nm, ca. 100 μJ) derived from the laser amplifier. By tuning the incident angle of these two beams relative to the crystal plane the sum frequency from the fluorescence light and the gate pulse was generated. The time resolved traces are then collected by detecting the sum frequency light, with a photomultiplier tube (R1527p, Hamamatsu) placed at the exit of a 30 cm monochromator, while changing the relative delay of the gate pulse versus the sample excitation time. The electrical signal from the photomultiplier tube was gated by a boxcar averager (SR 520, Stanford Research Systems) and detected through a lock-in amplifier (SR830, Stanford Research Systems). The prompt response of this arrangement (including laser sources) was determined by detection of scattered light under otherwise identical conditions and found to be approximately 100 fs (FWHM). This value was used in the analysis of all measurements for deconvolution of the upconversion data.

G. Photo-induced Absorption Spectroscopy.

The samples were prepared as spin-coated films onto the sapphire substrates and annealed for 15 minutes. Then, they were mounted in a nitrogen flow cryostat equipped with a temperature and pressure controller. The samples were cooled to 80 K and kept in vacuum during the measurements. As excitation light, a frequency-doubled continuous wave Nd:yttrium aluminum garnet (YAG) laser (λ_{exc}=532nm, P_{laser}=15mW) with a modulation frequency of 80 Hz was used and the transmission was probed with white light from a halogen tungsten lamp. Both sources were focused onto the same point of the sample and the diameter of the spot was 4 mm^2, corresponding to an intensity of 0.38 W/cm². The transmitted light was collected and focused into a monochromator by concave mirrors. The signal was then detected by a silicon detector in the wavelength range of 550-1100 nm (2.26 to 1.13 eV) and by an InSb detector in the range of 1100-5550 nm (1.13 to 0.22 eV) and recorded by a standard phase sensitive technique synchronized with the chopping frequency of the laser. The photo-induced absorption (PIA), corresponding to, $-\frac{\Delta T}{T}$, (where ΔT is the photo-induced change of the transmission and T the transmission of the sample) was plotted as a function of the wavelength of the probe light after correcting the change of transmission of the sample (ΔT) for the photoluminescence (PL) of the sample and then dividing by the transmission of the samples.[34,35] The PL correction measurements were done with the same setup. All the measurement results were finally normalized to the absorption of P3HT at the excitation wavelength (λ_{exc}).

H. Device Fabrication and Electrical Characterization.

The photovoltaic devices were prepared on glass/ITO substrates. First the substrates were pre-cleaned in an ultrasonic bath with Hellmanex detergent, deionized water, acetone and isopropyl alcohol, and treated in an ultraviolet-ozone chamber

for 30 minutes. A thin layer (~30 nm) of poly(3,4-ethylenedioxythiophene):poly(styrene sulfonate) (PEDOT:PSS, Baytron P VP AI 4083) was deposited onto the ITO glass by spin-coating at 3500 rpm for 60 s and then baked at 150°C for 15 minutes.

PbS QDs or a blend of P3HT:PbS QDs (90% loading of QDs) was dissolved in chloroform at a total concentration of 16-18 mg/ml.[11] The solutions were deposited on the PEDOT:PSS layer by spin-coating (1000 rpm for 60 s) to form a photosensitive layer. This was followed by the ligand exchange by 0.02 M BDT in acetonitrile[10]. Then the samples were rinsed with pure acetonitrile to remove the excess of BDT and OLA. Subsequently, to fill up the film cracks formed after BDT treatment, a thin neat QD layer was deposited onto the film by spin coating (1000 rpm for 60 s) from a solution of 5 mg/ml PbS:QDs in toluene. Then the ligand was exchanged and the sample cleaned as described above. All the films were subsequently annealed at 150°C for 10 minutes inside a nitrogen-filled glove box. Finally, the device fabrication was completed by the thermal evaporation of Ca (~20 nm) and Ag (100 nm) as a cathode.

The photovoltaic devices are measured inside a nitrogen filled glove box with a parameter analyzer (Agilent 4156C) or a Keithley 2602A under a 1000W Xe arc lamp equipped with filters to simulate the AM 1.5G spectrum (Abet). The lamp is calibrated using a Fraunhofer calibrated Si solar cell, equipped with a KG3 band pass filter. For the EQE measurements, light from Xe and quartz halogen lamps was coupled into a monochromator and the intensity was calibrated with a Si photodiode. The light incident on the device was chopped and the modulated current signal was detected with a lock-in amplifier coupled to the current-voltage analyzer. The same optics and measurement set-up was used in combination with with a DTR6-integrating sphere to determine the reflectance spectra (R, in %). The IQE values were determined as EQE/(100%-R)[12,28,36].

III. RESULTS AND DISCUSSION

A. Structure of P3HT:PbS blend films

Fig. 1 shows the TEM images of P3HT:PbS films with a loading of 60, 75, or 90% PbS before and after post-deposition ligand exchange by BDT. The measurement operated in bright field mode without energy filter and therefore the variations in image brightness could be due to thickness variation. In the low magnification images of the blend films containing PbS QDs with the initial OLA ligands (images a-c), one can see some irregular bright structures. These appear to be simply regions with a low concentration of quantum dots, as evidenced by the images at higher magnification (images d-f). The occurrence of such regions provides an indication for a certain tendency of the QDs to form aggregates in the film. Furthermore, the drying process can be responsible for those regions, because reduction of the volume of the film upon evaporation of the solvent can lead to the appearance of some cracks at nanometer length scales.

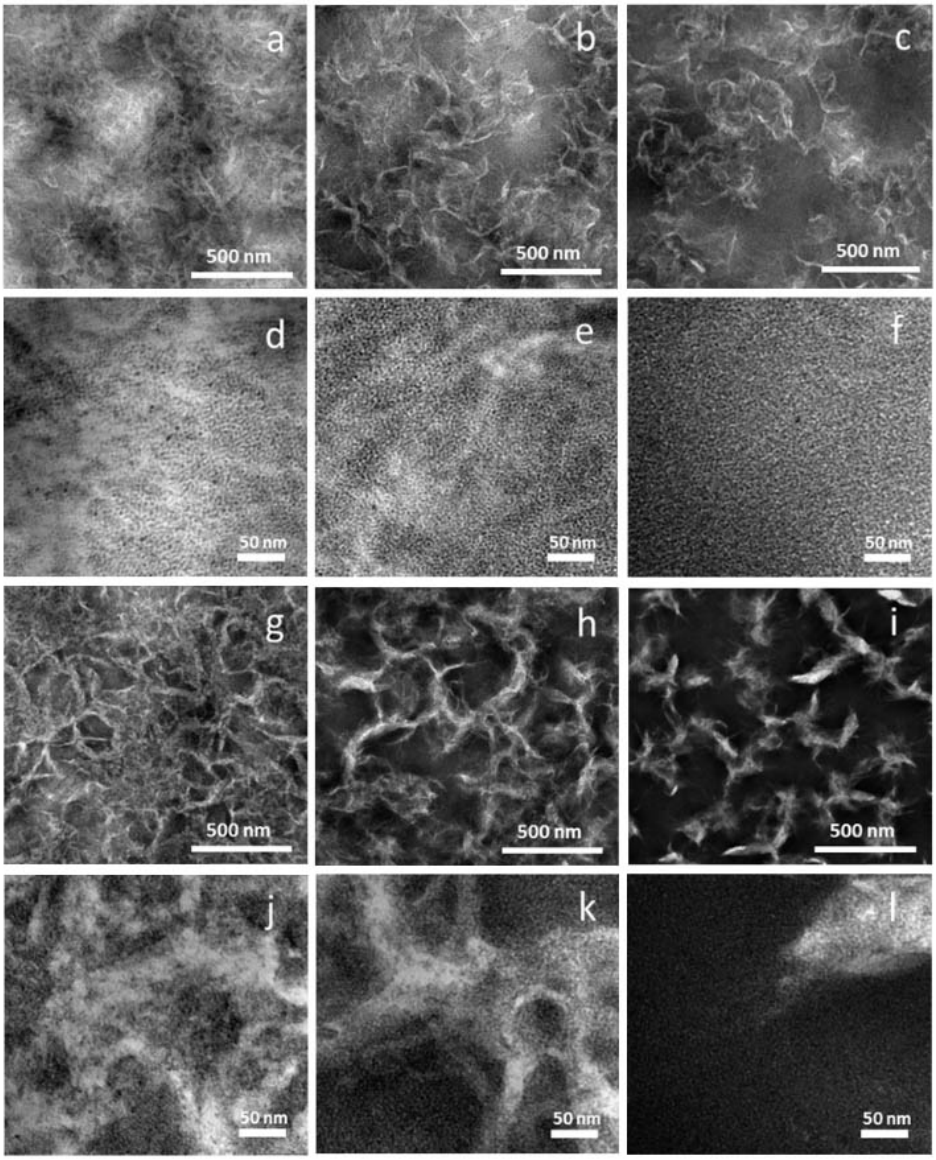

FIG. 1. (a)-(f) TEM images of P3HT:PbS-OLA blend films with different PbS loading (60% (a,d), 75% (b,e) and 90% (c,f)) at different magnification (scale bar is 500 nm (a-c) or 50 nm (d-f)). (g)-(l) TEM images of P3HT:PbS-BDT blend films with different PbS loading (60% (g,j), 75% (h,k) and 90% (i,l)) at different magnification (scale bar is 500 nm (g-i) or 50 nm (j-l)).

After the treatment of the films with BDT, the bright regions significantly increased (see images g-i). Again, high-magnification images (j-l) reveal that these regions are simply depleted of PbS QDs. At the same time, the other regions appear to contain QDs in a much more dense concentration. These observations provide good evidence for the success of the post-deposition ligand exchange with BDT as cross-linking molecule. Due to the cross-linking nature of, and smaller volume occupied by, this ligand, the PbS QDs are linked together and form denser structures. On the other hand, this means a reduction of the volume occupied by the QDs and therefore causes the appearance of regions with a low concentration of QDs between the aggregates.

The colloidal PbS QD capped by OLA exhibit a pronounced first excitonic absorption peak around 750 nm (see Fig. 2(a)), which corresponds well to a particle diameter around 2.4 nm according to established sizing curves.[37] Due to the size distribution, the absorption onset is observed around ~900 nm for the QDs used in this study. The steady-state optical absorbance of neat P3HT (solid lines) and the P3HT:PbS-OLA blend (dashed lines) films in the 400-1000 nm range is displayed in Fig. 2(b). The features of the spectra of neat P3HT are similar to those obtained earlier by ourselves[38] and other authors.[39-42] While between 500 and 600 nm the blend films with OLA capped PbS QDs show a similar absorption as the neat P3HT films, an increased absorption is found below 500 nm for the blend films. After BDT treatment, absorbance of the blend film increases between 400 and 500 nm by a factor of four in the sample P3HT:PbS-BDT 90% (while the increase is less pronounced in samples with a smaller loading of QDs). This increased absorption could be due to an increase of the dielectric constant upon replacing the OLA ligands by BDT ligands[43] or to an increased clustering of the QDs leading to an increased light scattering and hence optical path length. In addition, a broad and slightly red-shifted absorption peak, attributed to the first excitonic transition of the PbS QDs can be observed at ca. 650-900 nm for the sample with 90% PbS QDs. The features and the position of the maxima of fluorescence spectra (Fig. S1[29]) of films of neat P3HT and P3HT doped with PbS QDs (See SI, Fig S1 and S2[29]) are similar to those obtained earlier by ourselves[38] and by other authors.[39,41,44]

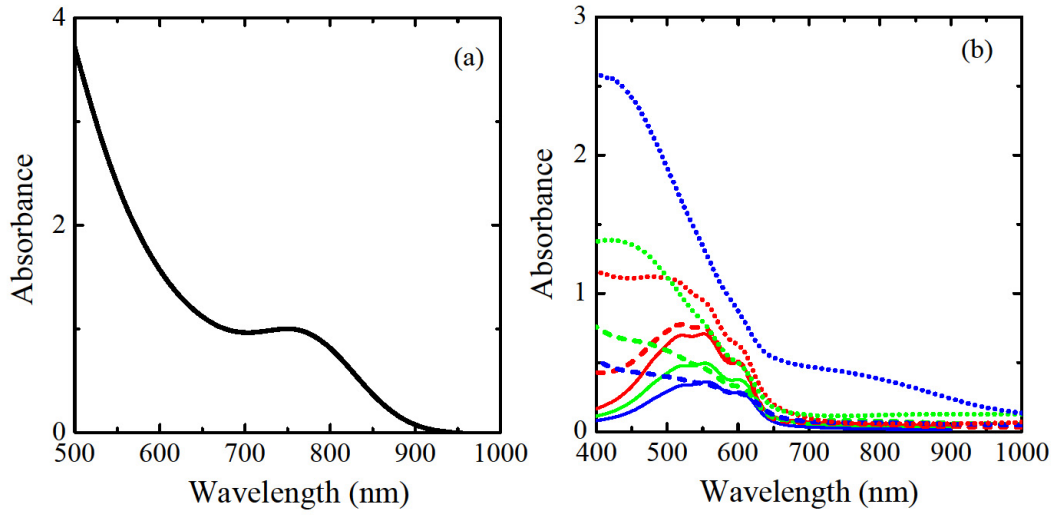

FIG. 2. (a) Absorption spectra of PbS QDs capped with OLA ligands in solution (toluene) (b) Absorption spectra of the P3HT:PbS film casted from chloroform (60% (red), 75% (green) and 90% (blue) of QDs). The QDs were capped with OLA ligands (dashed lines) and BDT ligands (dotteds line). The absorption spectra of P3HT films (solid line) casted from a solution with 8.5 mg/ml (red), 5.4 mg/ml (green), 3.8 mg/ml (blue)) correspond to the amount of P3HT present in the solutions used to cast the P3HT:PbS blends with 60, 75 and 90% QDs, respectively.

B. Time Resolved Photoluminescence

Electron transfer in donor-acceptor blends is expected to significantly reduce the fluorescence quantum yield of the donor phase which is suggested when comparing the emission spectra of neat P3HT to those of P3HT:PbS QD blends (Fig.

S1[29]) before and after exchange of the OLA ligands by BDT. The reduction of the intensity is clearly more pronounced after the ligand exchange. As at the wavelength where P3HT has to be excited there is a competitive absorption by the QDs it is difficult to determine the absorbance due the P3HT and hence the fluorescence quantum yield of P3HT accurately in the P3HT:PbS blends. This difficulty will be enhanced by the unexpected increased overall absorption upon ligand exchange to BDT (*cfr. supra*). Therefore, we preferred to determine the quenching of the P3HT emission by the QDs by time resolved fluorescence measurements using time-correlated single photon counting (TCSPC) and femtosecond up-conversion spectroscopy on neat P3HT and blend films of P3HT and PbS QDs (2.4 nm). The decays of the emission at 650 nm (1.91 eV) obtained by TCSPC upon excitation at 488 nm had to be analyzed as sum of two exponentials for films of neat P3HT and P3HT:PbS QD blends.

1. *Neat P3HT films*

In order to separate quenching by PbS from other decay channels and excited state relaxation processes a quantitative study of the quenching requires an understanding of the fluorescence decays of neat P3HT. The P3HT films were excited at 488 nm and the fluorescence decay detected at 650 nm (1.91 eV) (See Fig.3(a)) could be analyzed as a sum of two exponentials (Table I). The fast decaying component has a decay time close to the time resolution of the set-up (30-50 ps) and its amplitude decreases upon increasing the detection wavelength; at a detection wavelength of 750 nm (1.65 eV) the fluorescence decay becomes even mono-exponential (see Table S2[29]). The slow decaying component with a decay time of 671 ps, which is somewhat longer than the population decay time of 470 ps observed by Banerji *et al.*,[45] was attributed to the decay of the singlet excited state of P3HT by monomolecular non-radiative or radiative processes. One should note that the value obtained for P_2 (0.953) suggested that this component contributed more than 95% of the intensity recorded in the steady state and that its amplitude was increased at longer wavelengths (Table S2[29]) to the extent that the fluorescence decays became single exponential at 750 nm (Table S2[29]). As the short fluorescence decay-time recovered from the analysis of the fluorescence decays of neat P3HT as a bi-exponential decay is close to the time resolution of our set-up, it is possible that faster decaying components are overlooked in the analysis of the fluorescence decays by TCSPC. Therefore the fluorescence decays of P3HT at 650 nm, obtained upon excitation at 488 nm, were also investigated by fluorescence upconversion (FFU) where the fluorescence decay times can be determined with sub-picosecond time resolution in a time window of 30 ps and 400 ps. It was possible to analyze the decays obtained in both time windows as a sum of two exponentials while fixing the short decay time of the decay obtained in the 400 ps window to the value recovered for the long decay time from the decay obtained in the 30 ps time window. The analysis of the fluorescence decay at 650 nm of a neat P3HT film upon excitation of

488 nm obtained by FFU in a time window of 30 ps (Fig. 3(b)) yielded a fast component with a decay time of 310 fs and slower component with a decay time of 7.2 ps (Table II).

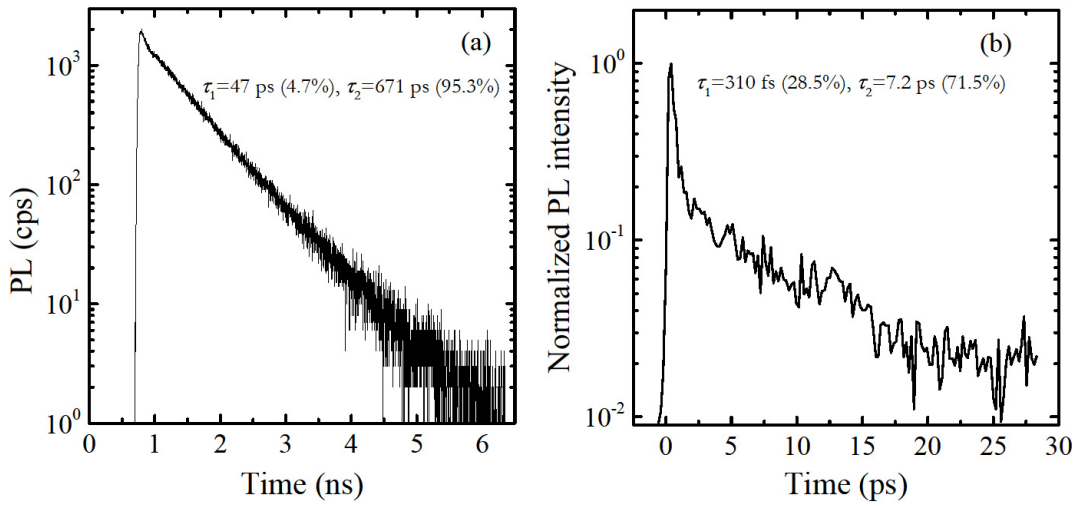

Fig. 3 Fluorescence decay (λ_{exc}=488 nm, λ_{em}=650 nm) of a neat P3HT film measured with (a) single photon timing (picoseconds time-resolved fluorescence) and (b) fluorescence upconversion (femtosecond time-resolved fluorescence for a 30 ps time window). Note that the number of photons $cm^{-2}pulse^{-1}$ was 10^6 times higher for the upconversion experiments. The contribution of the different components (P_1 and P_2) to the stationary emission at the detection wavelength are displayed at the top of the figures.

The dynamics of the initial photo-induced processes in P3HT films (the fluorescence decay components observed by FFU and the fast decaying component observed by TCSPC) can be attributed to several processes, including exciton localization, lattice relaxation, downhill relaxation of self-trapped excitons, torsional relaxation, excitation energy transfer (EET), singlet-singlet annihilation and singlet-triplet annihilation.[45,46–57] Exciton localization and downhill relaxation of self-trapped excitons can occur in less than 1 ps in oligothiophene and P3HT.[45,51,52] EET and torsional relaxation, although the latter could be restricted in solid films[54], in polymers and oligomers generally take place in a few ps to several tens of ps.[46,51,54,55,58] Singlet-singlet annihilation can be important in time resolved studies using high peak power femtosecond or picosecond pulses and has been reported to occur on a time scale from 3 ps up to several hundreds of ps in bulk films.[46,53] It has also been reported that only for average power less than 0.5 W/cm^2, the singlet-singlet and singlet-triplet annihilation will be negligible in bulk polythiophene films.[46] However experiments based on fluorescence microscopy of isolated chains or clusters thereof, where this process was suggested to be partly responsible for the reduction of fluorescence quantum yield (QY) at high excitation power (>0.1 W/cm^2), suggested a lower threshold and the presence of a "static" component besides the "dynamic" quenching.[50,59] The latter experiments also suggested a significant reduction of the fluorescence quantum yield (and hence an enhancement of the fluorescence decay rate) by the occurrence of singlet-triplet and singlet-polaron

annihilation at high excitation densities (> 0.1 W/cm²).[50,59,60] However, pump probe experiments and photo-induced absorption (*cfr. infra*) indicated that contrary to films of regiorandom P3HT or P3HT in solution, polarons rather than triplets are formed in regioregular P3HT films. [49,61–64] This is probably due to larger interchain interaction in highly ordered crystalline P3HT films leads to more efficient formation of polarons and polaron pairs than triplets. Hence if any exciton annihilation by long living species[46,59] occurs it will be rather by polarons than by triplets.

As in the TCSPC experiments the laser intensity used (9.6 mW/cm^2, ~2.8×10^9 photons/(pulse·cm^2)) was much below the expected onset of singlet-singlet annihilation at (10^{11} - 10^{12} photons/(pulse·cm^2)).[46–49] it is unlikely that the fast component observed in the analysis of the fluorescence decays obtained by TCSPC is due to singlet-singlet annihilation. The absence of "dynamic" quenching by singlet-singlet annihilation under those conditions was confirmed by the wavelength dependence of the normalized amplitude ($\frac{A_1}{\sum_i A_i}$) and the contribution (P_1) of this component, which even disappeared at 750 nm, and the observation that increasing the incident laser intensity to (27 mW/cm², 7.9×10^9 photons/(pulse·cm^2) still leads to a mono-exponential decay of the fluorescence detected at 750 nm without changing the decay time substantially (see Table S2[29]). The independence of the mono-exponential decay time of the 750 nm emission upon the laser intensity furthermore suggests that under the experimental conditions of the TCSPC experiments also "dynamic" exciton annihilation by long living species as triplets or polarons is not an important decay process.[46,50]

The dependence of the amplitude of the fast decaying component of the decays obtained by TCSPC on the emission wavelength and independence of the features of the decay at 750 nm on the laser intensity (Table S2[29]) suggest therefore that the fast decaying component observed by TCSPC is related to exciton relaxation.[45,46,51-53,54,55,58] Considering the time scale of the different fast relaxation processes mentioned above[45,46,51-53,54,55,58] torsional relaxation[54] or nearly iso-energetic energy transfer (EET)[45,46] to sections of the polymer chain (on the same chain or a neighboring one) emitting at slightly longer wavelengths (with *e.g.* a longer conjugation length, a better planarity or stronger exciton interaction with neighboring chromophores) are the most likely processes behind this decay component. In this case the fluorescence decay time of polymer segments emitting at shorter wavelengths will be decreased by the possibility of energy transfer while this decay channel will be closed for polymer segments emitting at longer wavelengths leading to a decrease of the normalized amplitude ($\frac{A_1}{\sum_i A_i}$) of the fast decaying component upon increasing the detection wavelength and the disappearance of this component at 750 nm (Table S2). Relaxation of the initially excited state by exciton localization, lattice relaxation or strongly downhill energy transfer (EET) to sections of the polymer chain (the same or a neighboring one) emitting at significantly longer wavelengths is less likely as those processes are expected to occur on a much shorter timescale (femtoseconds to a few picoseconds).[45,46,51,52]

In FFU experiments, where excitation occurs by pulses with energy between 0.1 and 0.2 μJ (corresponding to a laser power of 0.1 to 0.2 mW) the intensity of the incident laser pulses is for a beam diameter of 0.1 mm between $3.1x10^{15}$ photons $cm^{-2}pulse^{-1}$ and $6.3x10^{15}$ photons $cm^{-2}pulse^{-1}$ (1.3 $mJcm^{-2}pulse^{-1}$ and 2.6 $mJcm^{-2}pulse^{-1}$). This yields for an absorbance of the sample at the excitation wavelength of 0.4 and a thickness of the sample of 200 nm an initial exciton density of roughly $1-2\times10^{20}$ cm^{-3}. This is clearly in the range where both "static" and "dynamic" singlet-singlet, singlet-triplet and singlet-polaron annihilation are important. An exciton density of $1-2x10^{20}$ cm^{-3} means that the spatial separation is less than 2 nm for excitons generated in the laser focus. Although longer than the distance of 0.4 nm between neighboring assembled conjugated polymer chains, this distance is still sufficiently small to allow a rapid exciton-exciton annihilation.[51,53] Therefore, we assigned the decay of 7.2 ps in the neat P3HT film to a combination of EET to segments emitting at longer wavelengths and diffusion-limited singlet-singlet annihilation.[45,46,51,53] On the other hand, the observed 310 fs component can be attributed to the exciton localization and lattice relaxation of self-trapped (dynamic localized) excitons in neat P3HT films[45,46,51] assuming that charge transfer in neat P3HT can be ignored.[57]

2. Blend films of P3HT and PbS QDs

Fig.4 shows the decay of the fluorescence of P3HT measured with TCSPC for P3HT:PbS-BDT QDs blend films. As for a neat P3HT film the fluorescence decays could be analyzed as a sum of two exponentials. While the fast decaying component has in the blend films a decay time similar to that observed for the film of neat P3HT its normalized amplitude, $(\frac{A_1}{\sum_i A_i})$, is larger than in the neat P3HT film and increases systematically with the loading of PbS QDs (see Table I). Furthermore, in contrast to neat P3HT films the amplitude of this component is not decreased for fluorescence decays recorded at 725 nm. This suggests that in the blend films the fast decaying component is not only due to EET to chromophores emitting at longer wavelengths but also to quenching of the fluorescence of P3HT by the PbS QDs. The decay time of the slow decaying component and hence also the average decay time is decreased compared to neat P3HT films and decreases in a systematic way upon increasing the loading by PbS QDs (see Table I and Table S3[29]).

Although all fluorescence decays could be analyzed as a sum of two exponentials one cannot exclude that this is just an approximation of a more complex decay, especially in the blend films.[65] Therefore rather than using the individual decay times we determined the average decay time $<\tau>$ from the individual decay times (τ_i) and their amplitudes (A_i) using Eq. 1. This average decay time (Table II and Table S3[29]) decreases systematically upon increasing the load of PbS QDs (BDT) and shows except for the film of neat P3HT no significant dependence upon the analysis wavelength. In this framework the QY

of the quenching of the fluorescence of P3HT in blend P3HT:PbS-BDT films is given by $\left(1-\frac{\langle\tau\rangle_x}{\langle\tau\rangle_{P3HT}}\right)\times 100\%$, where $\langle\tau\rangle_x$ and $\langle\tau\rangle_{P3HT}$ denote the average PL decay times of the blend and neat P3HT, respectively (see Table I). While for blend films with PbS-OLA QDs (Table S3[29]) the values of <τ> were similar to those obtained for neat P3HT films, the values of <τ> obtained for blend films where the PbS QDs were capped by shorter ligands were significantly smaller (Table S3[29] and Table I). The efficiency of the fluorescence quenching amounted for a sample with 60% loading to respectively (65±2)%, (13±3)% and (45±5)% for blend films of P3HT with PbS-OAm, PbS-OT and PbS-BDT capped QDs. For the blend films with PbS-BDT QDs, the efficiency of the fluorescence quenching (Table I) increased to (56±3)% in films with a loading of 90% of PbS QDs (69 wt% of PbS QDs). As the decay time of the fast decaying component is close to the time resolution of the TCSPC set-up and as FFU experiments revealed the presence of faster decaying components for a neat P3HT film we also investigated the fluorescence decays of blend films with PbS-BDT QDs using FFU in a time window of respectively 400 and 30 ps (Figure 5). These decays could be analyzed as a sum of two exponentials (Table II). In order to be able to link the data obtained in the 400 ps time window to those obtained in the 30 ps time window, the decay time of the fast decaying component obtained for the fluorescence decays recorded in the 400 ps time window was fixed to the value of the decay time of the slow decaying component obtained for the fluorescence decays recorded in the 30 ps time window.

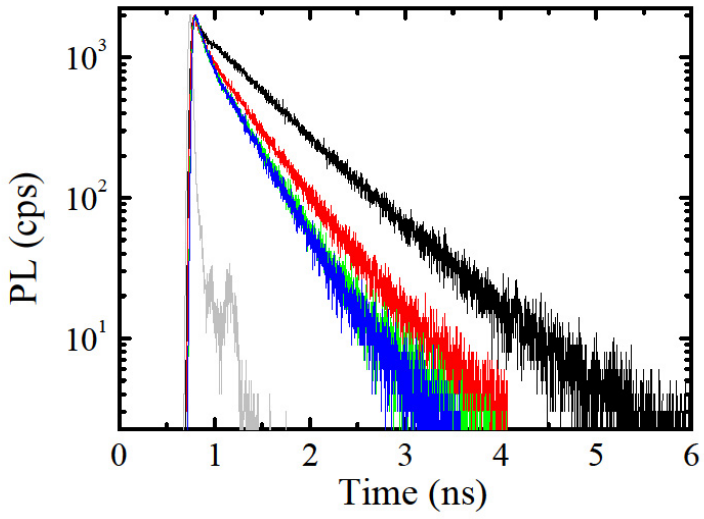

FIG. 4. Decays (λ_{exc}=488 nm, λ_{em}=650 nm) of the fluorescence of P3HT in a neat P3HT film (black line) and P3HT:PbS-BDT blend films (60% loading (red), 75% loading (green) and 90% loading (blue) by PbS QDs). The grey line corresponds to the instrumental response function (IRF).

TABLE I. Decay times (τ_i) and normalized amplitudes ($\frac{A_i}{\sum_i A_i}$) of the fluorescence of a neat P3HT film and blend P3HT:PbS-BDT films obtained using the TRFA global analysis program, $<\tau>$ is the average fluorescence decay time.

Samples	detection (nm)	$\frac{A_1}{\sum_i A_i}$	τ_1 (ps)	$\frac{A_2}{\sum_i A_i}$	τ_2 (ps)	$<\tau>$ (ps)	Efficiency of quenching by PbS QDs (%)	χ^2
P3HT	650	0.41	46.9	0.59	671	415	-	1.07
	725	0.27	37.6	0.73	680	507	-	1.06
+PbS-BDT 60%	650	0.52	56	0.48	470	255	39	1.1
	725	0.48	57	0.52	437	255	50	1.02
+PbS-BDT 75%	650	0.49	60.9	0.51	386	231	44	1.08
	725	0.48	61.9	0.52	379	223	56	1.01
+PbS-BDT 90%	650	0.56	50.4	0.44	366	189	54	0.98
	725	0.46	60.2	0.54	356	219	57	1.05

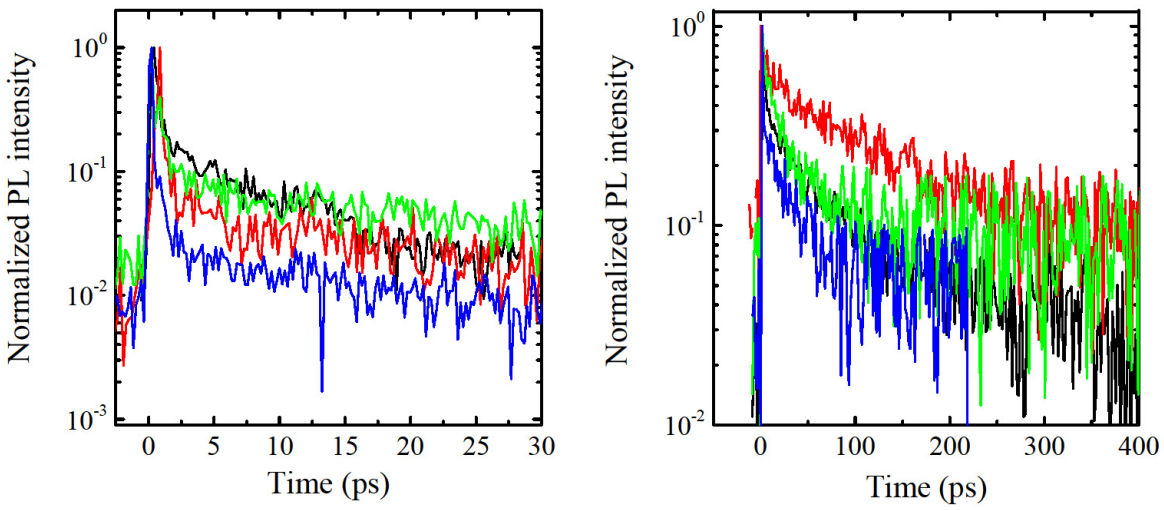

FIG. 5. Decays (in semilogarithmic scale) of the fluorescence of P3HT at 650 nm determined by fluorescence up-conversion for a film of neat P3HT (black line) and of P3HT:PbS-BDT 60% (red line), 75% (green line) and 90% (blue line) (a) time window of 30 ps (b) time window of 400 ps.

Upon addition of or increasing the load of PbS QDs the fast decay time is decreased from 310 fs in neat P3HT to 105, 118 fs and 55 fs (which is close to the time resolution of the set-up) in samples with respectively a loading of 60, 75 and 90% PbS QDs while the decay time of the intermediate component decreases from 7.2 ps in neat P3HT to 1.2 ps in P3HT loaded with 90% PbS-BDT QDs. A similar observation can be made for the decay time of the slow decaying component observed in the 400 ps window (Fig. 5(b)) which decreases from nearly 93 ps in neat P3HT and P3HT with a 60% loading of PbS-BDT QDs to 31 ps in a sample with a loading of 90% of PbS-BDT QDs.

TABLE II Decay times (τ_i) and normalized amplitudes ($\frac{A_i}{\sum_i A_i}$) of the components of the fluorescence decay of P3HT at 650 nm obtained by FFU for a neat film of P3HT and P3HT:PbS-BDT 60%, 75% and 90% blend films (fitted to a bi-exponential decay). The normalized amplitudes ($\frac{A_i}{\sum_i A_i}$) of the different components of the decay were obtained by combining the decays obtained in the 30 ps and 400 ps time window. In the analysis of the fluorescence decays recorded in a time window of 400 ps the decay time of the fast decaying component was fixed to the value of the decay time of the slow decaying component obtained in the analysis of the fluorescence decays recorded in a time window of 30 ps.

Samples	*time window* *(ps)*	$\frac{A_1}{\sum_i A_i}$	τ_1 (ps)	$\frac{A_2}{\sum_i A_i}$	τ_2 (ps)	$\frac{A_3}{\sum_i A_i}$	τ_3 (ps)	χ^2
P3HT	30	0.88	0.31	0.09	7.2	-	-	0.98
	400	-	-	0.09	7.2	0.03	92.6	0.93
+PbS-BDT 60%	30	0.93	0.105	0.02	5	-	-	0.94
	400	-	-	0.02	5	0.05	92.5	0.74
+PbS-BDT 75%	30	0.85	0.118	0.08	2	-	-	0.93
	400	-	-	0.08	2	0.07	27.2	0.83
+PbS-BDT 90%	30	0.98	0.055	0.017	1.2	-	-	0.99
	400	-	-	0.017	1.2	0.003	31.3	0.9

Recent work on ultrafast exciton quenching showed that increasing the concentration of regioregular P3HT in poly(methyl methacrylate) (PMMA) matrix increased the photo-induced quenching at high excitation power density.[50] As the increase of the loading by PbS QDs also means dilution of the P3HT chromophores in the blends it can be expected to decrease rather than increase the rate of the different exciton annihilation processes. Hence the decrease of the decay times of the fast and intermediate components upon increasing the loading of PbS QDs can be attributed to ultrafast quenching by the PbS QDs, and as at the same time exciton annihilation is partly suppressed the observed changes of the decays even underestimate the ultrafast quenching by PbS QDs. This means that the quenching of the singlet state of P3HT by the PbS QDs, probably (*cfr. infra*) by charge transfer, occurs on a time scale ranging from tens of fs to a few hundred of ps. This broad range of decay times (which probably reflects a non-exponential decay) is due to the fact that the fast (fs) charge transfer can only occur between P3HT chromophores adjacent to PbS QDs; for P3HT chromophores at a larger distance from the QDs the charge transfer has to be preceded by exciton hopping. The necessity of exciton hopping in spite of the high loading of PbS QDs suggests an extensive phase separation between P3HT and PbS QD domains in the blend films and heterogeneous nature of the samples (*cfr. supra*) as also shown in Fig. 1(g) –1(l). The combination of exciton hopping to a chromophore close to a QD followed by energy or electron transfer of the QD also means that the decay time τ_1, obtained from the FFU experiments rather than $<\tau>$ estimated from the TCSPC experiments corresponds to the electron or energy transfer form a chromophore adjacent to the QDs, to the QDs. Although the complex nature of the decays (especially considering the occurrence of exciton annihilation in the FFU-experiments) makes it impossible to combine the decay

parameters obtained by FFU and TCSPC and to get a quantitative evaluation of the efficiency of the charge transfer, the fluorescence quenching observed in the FFU experiments on blend films with PbS-BDT QDs suggests that the efficiencies for the quenching by PbS QDS obtained from the analysis of the TCSPC data are a lower limit as the latter do not consider the ultrafast quenching processes.

One should note that FFU experiments yielded for a blend film with PbS-OLA QDs (60% loading) a short decay time of 520 fs which is even longer than the value found for neat P3HT (Fig S3[29]). The increase of the decay time of the fast decaying component from 310 to 520 fs could perhaps indicate a reduced exciton annihilation due to dilution of the P3HT chromophores by the PbS-OLA QDs. The data obtained by FFU for the sample with PbS-OLA QDs agree with the fluorescence decays of this sample obtained by TCSPC which indicate that no fast quenching by PbS QDs takes place (Table S3[29]).

The quenching of P3HT by PbS QDs can in principle occur by charge transfer and by energy transfer. On one hand P3HT and 2.4 nm PbS QDs form a good type II heterojunction while on the other hand (Fig. S2[29]) the absorption of the PbS QDs overlaps very well with the emission of P3HT. Fig. S2 shows that the dependence of the intensity of the PL of the PbS-OLA QDs on the excitation wavelength reflects the absorption spectrum of the neat film of PbS-OLA QDs, where light absorption is only due to the QDs rather than the absorption spectrum of the blend films where part of the light is absorbed by P3HT. This indicates that only direct excitation of the QDs results in PL of the QDs and that even at loading of 90% by the PbS-OLA QDs no major energy transfer from P3HT to PbS-OLA QDs occurs. Although PbS QDs treated with 1,3 benzenedithiol (1,3 BDT) showed PL in other studies[66,67], we did not observe a PL signal in our work with 1,4-BDT ligands. In this respect it is important to note that also for PbS QDs treated with 1,4 butanethiol ligands[68] no PL was observed at room temperature. Therefore, it is not possible to confirm or exclude energy transfer to the PbS QDs in P3HT:PbS-BDT blend films. Assuming a similar spectral overlap and oscillator strengths we can however estimate the ratio of the rate constants for Förster transfer[69-71] from a neighboring P3HT chromophore to PbS-OLA, PbS-OT and PbS-BDT QDs. The average radii of the QDs including the ligand shell amount to 1.75 nm, 1.93 nm, and 2.27 nm for respectively PbS-BDT, PbS-OT and PbS OLA QDs. If we take these values as distance between the center of the QD and the closest P3HT chromophore the ratio of the rate constants for energy transfer is 4.7 and 1.8 between PbS-BDT and PbS-OLA or PbS-OT respectively. The average thickness of the ligand shell is in this case 0.55 nm, 0.73 nm, and 1.07 nm for PbS-BDT, PbS-OT and PbS-OLA QDs respectively. The distance dependence of the rate constant for electron transfer, k_{et}, which requires orbital overlap[72-73] between the LUMO of P3HT and the CB of the PbS QD can be approximated by $k_{et} \propto \exp(-\beta R)$ with β between 0.8 an 1.2 $Å^{-1}$ (for R in Å)[73] or by $k_{et} \propto J^2$ (where J is the electronic coupling matrix element) and $J \propto \exp(-0.72R)$ (with R in Å)[75] This

would mean that k_{et} would increase by a factor of 65 to 1880 when the thickness of the ligand shell is decreased from 1.07 nm (PbS-OLA QDs) to 0.55 nm (PbS-BDT) QDs. Decreasing the thickness of the ligand shell from 0.73 nm (PbS-OT) to 0.55 nm (PbS-BDT) would increase the rate constant for electron transfer by a factor 4 to 14. Actually the difference will be even larger as due to the presence of π- and π*-orbitals the barrier for electron tunneling and hence the value of β will be smaller for BDT than for OLA-ligands.[72-76] These estimates indicate that the thicker shell of the OLA ligands will rather block electron transfer[72-76], than energy transfer by a Förster type mechanism[69-71]. The absence of quenching when P3HT is blended with OLA capped PbS QDs and the strong quenching by PbS-BDT suggests therefore that the quenching in P3HT:PbS-BDT blend films is due to electron rather than energy transfer.

C. Photo-induced Absorption

In order to check further whether the quenching of the PL of P3HT by PbS QDs is caused by photo-induced electron transfer between P3HT and the PbS QDs, photo-induced absorption (PIA) experiments were performed. The PIA spectrum of a neat P3HT film, which is given in Fig. 6(a), shows contributions from photo-induced absorption (positive signals) and from photobleaching (negative signals). The negative signal around 2.0 eV, of which the features match the low temperature absorption spectrum of P3HT, corresponds to a fingerprint of the photobleaching bands of P3HT.[77,78] Furthermore, the PIA spectrum of neat P3HT exhibits three main absorption peaks in the near infrared and visible region at 1.05eV, 1.24eV, and 1.83eV, respectively. Beek *et al.*[78] attributed the peak at 1.05 eV to the triplet-triplet absorption of P3HT which would suggest that a fraction of the singlet excitons created by light absorption decay by intersystem crossing. This assignment is supported by the large amplitude of the signal, which is only compatible with a species living several hundreds of microseconds (μs) up to milliseconds (ms), a condition necessary to reach a sufficient pseudostationary concentration (see SI[29]). However, in the literature, no further indications of triplet exciton formation in films of regioregular (RR) P3HT were found[61-64], e.g. transient absorption spectra rather suggested the efficient formation of polarons.[61–64] In solution, where intersystem crossing in P3HT is more efficient, the T_1-T_n absorption of P3HT was observed but this band was situated at higher energy, between 1.25 and 1.5 eV.[61] Furthermore, the band at 1.05 eV was not observed by PIA detected magnetic resonance measurements, which suggested that it should be attributed to a singlet (no net spin) species.[63,64] and prompted the assignment to a spin-singlet interchain exciton.[63,64] Such interchain singlet exciton would correspond to an electron and hole located on different polymer chains and bound by Coulomb interaction.[79] In such species the correlation between the electron and the hole, necessary to have a singlet rather than two uncorrelated doublets, would require a relatively short (maximum a few nm) distance between the electron and the hole.[80–82] Also the difference between the position of this signal and those attributed to the polarons (*cfr. infra*) suggests a strong Coulomb interaction and a small distance of maximum a few nm

between the electron and the hole. Hence one would expect that recombination to the ground state would occur in the nanosecond time range in such species. This would lead to a small pseudostationary concentration of this species (see SI) which is not compatible with the large amplitude of the PIA signal. Thus, the origin of the peak at 1.05 eV remains controversial and taking into account all arguments it should be attributed tentatively to a long living singlet species of unknown nature.

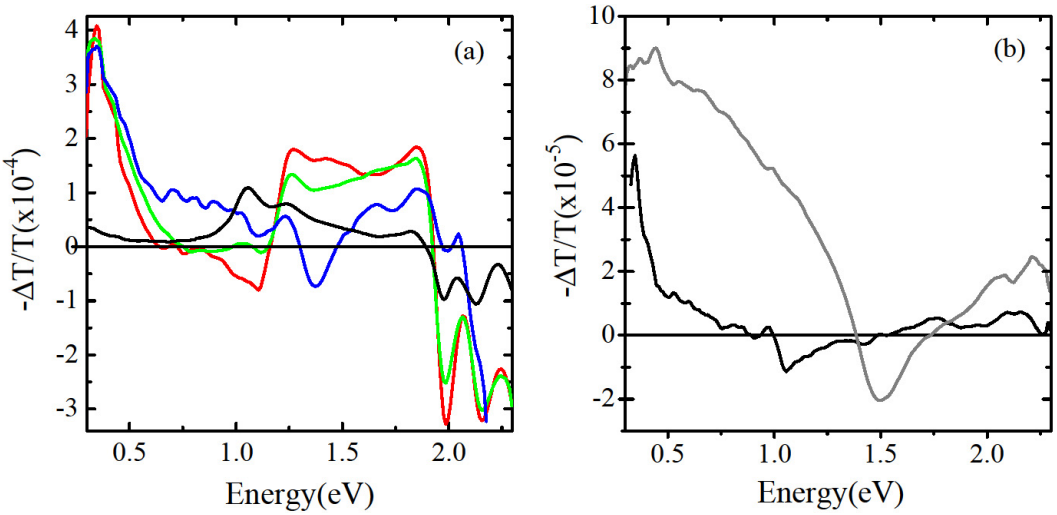

FIG. 6. (a) PIA spectrum of neat P3HT (black) and P3HT:PbS-BDT 60% (red) 75% (green) and 90% (blue) blend films. (b) PIA spectrum of neat PbS films capped by OLA ligands (black) and after treatment with BDT (grey).

The peaks at 1.24 eV and 1.83 eV are characteristic of polarons (cation radicals) generated in P3HT.[62–64,77,83] One should note that the second band is generally observed at slightly smaller energies 1.70 eV[63,64,77] or 1.75[83] eV. However this energy range corresponds also to the PL maximum of P3HT and is very sensitive to a proper correction of the PIA spectra for the photoluminescence. The signal at 1.24 eV (P_2) is assigned to a dipole-allowed transition between polaronic levels located in the HOMO and LUMO gap of the neutral polymer[63,64,77] (or the SOMO (semi-occupied molecular orbital, see Fig. S4[29]) to LUMO transition of a positive polaron[62,83,84]). The band at 1.83 eV (DP_2) is generally assigned to the same transition in a delocalized polaron state.[63,64,77] However Sirringhaus *et al.*[83] attributed this band, also observed in electro-absorption experiments, to the transition from the SOMO to a higher unoccupied orbital in a positive polaron.[85] The different assignments of the polaron bands are related to whether the signals are interpreted in the framework of semiconductor physics[63,64,77] or in analogy with the spectra of radical cations of oligothiophenes[62,83,84]. Besides the singlet band and the P_2, and DP_2 bands also a bands at lower energy (0.35 eV and 0.06 eV[63,64] or 0.2 eV[83]) were observed in the literature which were attributed to P_1 transition from the HOMO of P3HT to the lowest polaron level in respectively localized (P_1) and delocalized (DP_1) polarons.[63,64,77] In an alternative approach these transitions were attributed to or to a transition from the HOMO to the

SOMO (P_1) and an interchain CT transition between the HOMO of a neutral polymer chain and the SOMO of a positive polaron (DP_1).[83,84] Although the formation of localized and delocalized polaron states has a quite low efficiency for band gap excitation,[86,87] except for high intensity pulsed laser excitation, their long lifetimes can lead to an appreciable pseudo-stationary concentration. Under the experimental conditions used here the excitation occurred at 2.33 eV which is about 0.4 eV above the band gap, corresponding to the optical transition to the zeroth vibrational level of the P3HT singlet exciton (1.95 eV in the absorption spectrum), and could explain enhanced formation of polarons.[86–88]

In general, the ligand exchange of OLA ligands to BDT ligands on PbS QDs caused a vanishing of the signal of the singlet species at 1.05 eV while the signals attributed to the localized (P_2) and delocalized polaron (DP_2) and the ground state depletion became more pronounced (Fig. S6[29] and Fig 6(a)). This could suggest efficient electron transfer from P3HT to the PbS QDs. Similar features can also be observed in the PIA spectrum obtained for a blend of P3HT with 50% of PCBM (Fig. S5[29]). Increasing the concentration of PbS-BDT QDs slightly reduced the intensity of the signal corresponding to the polaron state (P_2), the delocalized polaron state (DP_2) at 1.8 eV and the broad band between 1.3 and 1.6 eV. Furthermore, for these samples the PIA spectra also showed a pronounced positive band with a maximum at 0.35 eV, which could be attributed to the P_1 transition. However, Zhang *et al.*[89] reported PIA spectra of neat PbS QD films which showed a broad band in the infrared region around 0.43 eV at 10 K for QDs of comparable size as used in this study. They attributed this band to a transition from a below-gap state to the second excitonic level of the QDs. However, the comparison between PIA spectra of the blend films and neat PbS-OLA and PbS-BDT films shown in Fig. 6 and Fig. S6[29] clearly show that the increase of the bands at 0.35, 1.24 and 1.83 eV can be attributed to charge transfer between P3HT and PbS-BDT QDs. In the 90% sample we also find a relatively broad absorption between 1 and 0.6 eV. As a similar band was found in a layer of neat PbS-BDT QDS (Fig 6(b)) this signal could be attributed to charges in the PbS QDs.

Contrary to the P_2 and DP_2 signals and the broad band at 1.36 eV, the signals attributed to the ground state depletion and the P_1 absorption are less affected by the loading by PbS QDs. At first sight, this appears contradictory to the fluorescence quenching experiments that suggest more quenching and hence formation of polaron pairs by charge transfer. This discrepancy could be explained by an increase of the rate of polaron recombination upon increasing the loading of PbS QDs. If both the rate of polaron generation and decay are enhanced to a similar extent upon increasing the loading, the pseudo-stationary concentration of polarons and the intensity of the corresponding PIA signals will not change extensively.

Note that, for the blend films with 60% loading of PbS QDs exchanging (in solution) the OLA ligands by OAm and OT results in a slight decrease of the singlet absorption peak at 1.05 eV (Fig. S6) whereas the depletion at higher energy is quite

similar for on one hand P3HT blended with PbS-OLA QDs and on the other hand P3HT blended with PbS-OAm or PbS-OT QDs. Contrary to the PIA spectra, the time resolved fluorescence quenching experiments on the P3HT:PbS-OAm blend films using TCSPC showed the most extensive quenching of all samples (*cfr. supra*). The absence of polaron signals could then suggest that fluorescence quenching occurs by energy transfer rather than by electron transfer or that electron transfer is followed by a very fast recombination. Note that ligand exchange of PbS QDs to OAm led to a structural change (nanorod formation, see Fig. S7[29]) and that a P3HT film doped with 36% of PbS QDs (OAm) showed a decrease of the hole mobility around one order of magnitude compared to P3HT films doped with PbS-OLA of the same loading.[38,90] In this respect the PIA signals rather than the extent of fluorescence quenching match the influence of the ligands on the PCE of hybrid PVs of P3HT and PbS QDs.[11]

D. Photovoltaic Devices

In agreement with the PIA experiments the most efficient photovoltaic devices obtained for blend P3HT:PbS QD films are those with BDT ligands (PCE ~0.9%).[11] By deposition of a extra neat PbS-BDT QD layer on top of the P3HT;PbS-BDT bulk heterojunction the average photovoltaic efficiency of a P3HT:PbS-BDT 90% photovoltaic device could be increased in the present work up to (1.8±0.25)% with the efficiency of the champion solar cell yielding a PCE of 2.17% (J_{SC}=9.5 mA/cm^2, V_{OC}=0.56 V and FF=40.6%) (See Table III). This is considerably larger than the PCE value (0.84±0.05) obtained for the corresponding device[11] without the neat PbS-BDT QD layer. This increase of the PCE compared to Ref.11 is attributed to a decrease of the leakage current as shown by the higher shunt resistance compared to the previously reported devices (Table S4[29]) and is also reflected in an increase of the open circuit voltage and fill factor from respectively (0.35±0.02) V and (33±0.8)% to (0.51±0.03) V and (40.4±1.5)% (Table III).[29] The larger leakage current in the previously reported devices was probably due to the film cracks observed in TEM images (Fig. 1). These cracks are often observed after the replacement of bulkier ligands as OLA with smaller ligands such as BDT.[91]

TABLE III. Average photovoltaic performance values of P3HT:PbS-BDT 90% and neat PbS photovoltaic devices build up in following way: (ITO/PEDOT:PSS/active layer/PbS-BDT (5 mg/ml)/Ca/Ag). Thereby, the active layer consisted of P3HT:PbS (90%) or PbS only, and was treated with BDT. The current voltage plots of the devices were obtained under AM1.5G filtered spectral illumination (100 mW/cm^2). J_{SC}, V_{OC}, FF and PCE are, respectively, the short circuit current density, the open-circuit voltage, the fill factor, and the power conversion efficiency. (Values in the brackets are the best values recorded).

Samples	thickness (nm)	J_{SC} (mA/cm^2)	V_{OC} (V)	FF (%)	PCE (%)
P3HT:PbS-BDT 90% [a]	160	7.2±0.1 (7.2)	0.35±0.02 (0.37)	33±0.8 (34)	0.84±0.05 (0.91)
P3HT:PbS-BDT 90%	130	8.6±0.57 (9.5)	0.51±0.03 (0.56)	40.4±1.5 (40.6)	1.8±0.25 (2.17)
PbS-BDT	120	9.1±0.45 (10)	0.52±0.03 (0.58)	44±2 (47.5)	2.1±0.3 (2.75)

[a] Structure of the photovoltaic devices: ITO/PEDOT:PSS/active layer/Ca/Ag, i.e., without an additional PbS layer deposited on top of the active layer.[11]

In order to further elucidate the mechanism of excited state electron transfer from P3HT to the PbS QDs in the PVs we also investigated a photovoltaic device where the active layer consists of a neat layer of PbS QDs with BDT ligands. The PCE of this device amounted to (2.1±0.3)% (average) while a PCE of 2.75% (J_{SC}=10 mA/cm^2, V_{OC}=0.58 V and FF=47.5%) (Table III) was obtained for the best device.

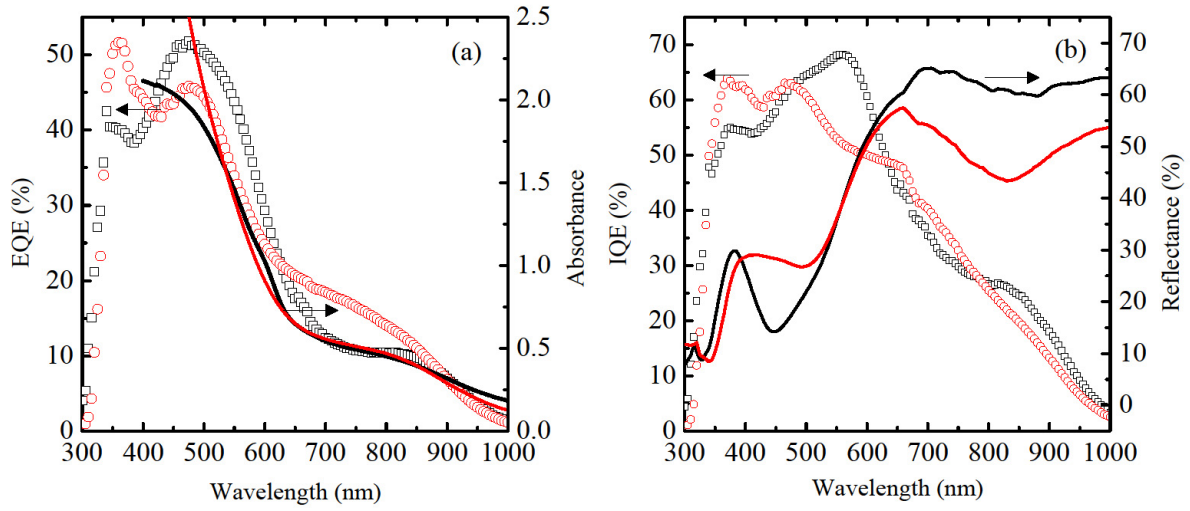

Fig. 7: Wavelength dependence of (a) the external quantum efficiency (EQE) and (b) internal quantum efficiency (IQE) of P3HT:PbS-BDT 90% (□) and neat PbS-BDT (○) photovoltaic devices. Fig. 7 also shows (a) thin film absorption spectra and (b) reflectance spectra of the active layer of P3HT:PbS-BDT 90% ——— and neat PbS-BDT ———. The absorption spectra (Fig. 7(a)) were measured for a thin film of the active layer spin coated on a glass substrate and prepared under similar conditions as that of the photovoltaic devices. The reflectance spectra (Fig. 7(b)) were determined for a complete photovoltaic device. The IQE was estimated by dividing the EQE spectrum by the absorbance of each device as obtained from the reflectance spectra.

Table III shows that the increased PCE of the device with the neat PbS-BDT QD layer is mainly due to an increase of both the short circuit current density (J_{SC}) (by 5%) and the fill factor (FF) (by 10%). The increase of the fill factor is reflected in the smaller series resistance (R_S) and an ideality factor closer to one, obtained from the analysis of the plot of the dark current (Fig. S8, Table S4[29]) versus the voltage. The larger value of FF and the smaller value of R_S could suggest a better carrier transport. As this device contains no bulk heterojunction with the electron donating polymer P3HT the photocurrent has to be generated mainly by direct separation of the electron-hole pair in the QDs. This is most probably caused by band bending near the metal contacts (Schottky diode).[23,24] The latter process will be quite efficient as the thickness of the device (120 nm) is less than width of the depletion layer formed in similar devices.[12,28]

The larger J_{SC} of the device with a neat layer of PbS-BDT QDs (which is reflected in the larger external quantum efficiency (EQE) between 620 and 850 nm, see Fig. 7(a)) could be due to higher absorbance in this wavelength range, a less efficient charge carrier recombination and/or more efficient charge carrier generation compared to the devices with

P3HT:PbS-BDT QD blend. As due to interference effects the actual light absorption and its wavelength dependence can be different in a complete solar cell compared to an active layer of the same thickness and composition deposited on a glass substrate, we also measured the reflection spectrum of the solar cells. Assuming that all light that is not reflected was absorbed by the active layer, which is a reasonable assumption between 450 and 1000 nm[12,28,36], the internal quantum efficiency (IQE) and its wavelength dependence (Fig 7(b)) could be calculated from the reflection spectra and the EQE. The reflectance spectra of the blend film and the neat PbS-BDT QD layer in Fig. 7(b) show that the larger EQE observed for the latter device between 620 and 850 nm (Fig 7(a)) is due to more efficient absorption of photons in this wavelength range. As the solar spectrum has a high intensity in this wavelength range this can also explain the increased J_{SC} observed for the solar cells with only an active layer of neat PbS-BDT QDs.

As in the device with a neat PbS layer direct separation of the electron hole-pair in the QDs leads to photocurrent generation one could wonder whether this process will also occur in the P3HT:PbS-BDT 90% device, where the volume fraction of P3HT is only 19%, and whether this process would generate in this device the photocurrent with a higher efficiency than electron hole separation at the interface between P3HT and the QDs. Figure 7(b) suggests this is not the case as the IQE for excitation in the first exciton band of the PbS QDs is clearly smaller than that for excitation of P3HT between 480 and 600 nm, where the polymer absorbs a large fraction of the incident light. Although the different trends for the wavelength dependence of the IQEs were observed in PVs with a neat QD layer[36] these effects only occurred in thicker devices where the width of the depletion layer was smaller than the thickness of the device. As this is not the case here one does not have to take into account this effect for our device with the neat QD layer. The observation that the IQE of the hybrid P3HT:PbS-BDT QD device is larger for excitation in the absorption band of P3HT than for excitation in the first excitonic band of the QDs suggests that a larger rather than a smaller fraction of the absorbed photons is converted into free electrons and holes via electron transfer from P3HT to the PbS QDs in the blend films compared to direct exciton dissociation in the PbS QDs in these films. If energy transfer from P3HT to the QDs followed by exciton dissociation in the QDs would be the major charge generating process one would expect a similar or even smaller IQE (as the efficiency of the energy transfer is less than 100%) upon excitation in the P3HT absorption band compared to excitation in the first excitonic band of the QDs. The increase of the IQE at shorter wavelengths in the PV with only a neat layer of PbS-BDT QDs the IQE could be due to a more efficient photodissociation of hot excitons[28,36] or multiple exciton generation[12]. As the onset of the increased IQE already occurs at energies much smaller than three times the band gap of the QDs the former mechanism is the most plausible one.

A fourfold increase of the short circuit current (J_{SC}) was observed in PVs based on blend films of P3HT and PbS-BDT QDs when the loading by the QDs was increased from 60% to 90%.[11] The same increase of the loading increased in these blend films the efficiency of fluorescence quenching (as determined by TCSPC) and hence of photo-induced electron transfer only from 45% to 56%. As the efficiency of fluorescence quenching obtained by TCSPC should be considered as a lower limit and as the fluorescence quenching efficiency can never be larger than one it cannot in the best case increase by a factor of two when the loading by PbS QDs is increased for 60% to 90% in blend films of P3HT and PbS-BDT QDs. The increase of J_{SC} upon increasing the loading suggests that upon increasing the loading also the efficiency of recombination was decreased. The intensity dependence of J_{SC} indicated that under these conditions (short circuit) and light intensities below AM1.5G recombination occurred by mainly by geminate and trap-assisted recombination, especially in devices with 60% and 75% loading of QDs.[43] At higher light intensities or at a loading of 90% also Langevin type non-geminate recombination can become important. While increasing the loading of PbS-BDT QDs from 60% to 90% increased the electron mobility significantly, the hole mobility was only slightly decreased.[43] This increased carrier mobility could lead to a faster escape of the hole or electron from the initially formed geminate electron hole pair and hence to a decreased efficiency of geminate recombination. This could explain why increasing the loading led to stronger increase of the values of J_{SC} compared to the fluorescence quenching.

For the device with a blend P3HT:PbS-BDT QD film with 90% loading the maximum value of the IQE for excitation of P3HT amounted to 50% (Fig. 7). As the efficiency of photo-induced electron transfer is between 56 and 100% in this device the efficiency of carrier recombination is under short circuit conditions between zero and 44%. In devices with a lower loading of PbS QDs a more extensive recombination will occur under short circuit conditions.[11,43]

IV. CONCLUSIONS

In line with earlier experiments,[90] we observed that the efficiency of the quenching P3HT by PbS QDs with different ligands increased when the average thickness of the ligand shell decreased from 1.07 nm (OLA) over 0.73 nm (OT) to 0.55 nm (BDT). This trend is also found in the PIA signals (polaron absorption and ground state depletion in P3HT) and in the PCE of PVs using P3HT blends with PbS QDs with different ligands[11]. For PbS QDs with OAm ligands in spite of a thicker shell (0.71 nm) the most efficient quenching was observed. This deviation from the trend found for the other ligands could be related to structural changes (Figure S7[29]) of the QDs induced by exchange of the OLA ligands to OAm ligands. For the latter combination, the increased quenching does however not lead to enhance polaron absorption in the PIA experiments or an enhanced PCE of the corresponding PV.[11] One should note that upon ligand exchange to OT, OAm and BDT ligands the

increase of the PCE[11] (up to three orders in magnitude) than the increase of the efficiency of fluorescence quenching. This due to fact that decreasing the thickness of the ligand shell will probably also increase the electron mobility and the efficiency with which the photogenerated electrons are collected the collection of electrons at the anode.

Combining the TCSPC experiments with FFU experiments showed that the quenching occurred over a broad time range including components in the order of tens of femtoseconds to hundreds of picoseconds. Even for samples with a 90% loading by PbS-BDT QDs (where only 19% of the volume of the sample is occupied by P3HT) still a component decaying with a decay time of more than 350 picoseconds is observed. For this sample the concentration of PbS QDs amounts to 6.0×10^{2} M, considering a volume fraction of 26.1% of PbS for and a volume of 7.23×10^{-21} cm^3 for a PbS-core and assuming that no clustering occurs. This means that the average distance between two QDs is 3.75×10^{-9} m, assuming a homogeneous distribution. Under these conditions the maximum distance of a P3HT segment to the edge of a PbS QD (which has a radius of 1.2×10^{-9} m) amounts to 6.8×10^{-10} m. In this case it is unlikely that for an important fraction of the P3HT chromophores the fluorescence decay time is not shorter than 350 ps. Therefore, the decays suggest an inhomogeneous sample where the PbS QDs are clustered which will lead to a number density of clusters that is smaller than that of individually distributed PbS QDs and hence results in (Figure 1) P3HT chromophores at a considerable distance (too long for electron transfer or direct energy transfer) from the edge of the nearest QDs. For these chromophores some residual quenching occurs by exciton hopping to chromophores close to the QDs followed by energy or electron transfer from these chromophores to the QDs. Such process will lead to a non-exponential fluorescence decay spanning a broad range of time scales.[92] The PIA experiments as well as the electro-optical characterization of the PVs showed that this quenching eventually led to the formations of positive polarons on the P3HT chain. The strong dependence of the quenching upon the thickness of the ligand shell, the absence of energy transfer in P3HT blended with PbS-OLA QDs and the wavelength dependence of the IQE suggest that the quenching and resulting formation of polarons occurs rather by electron transfer than by energy transfer to the QDs followed by exciton dissociation in the QDs. The decay time of the fast decaying component (50 to 100 fs) observed in the FFU experiments indicates that this photo-induced electron transfer occurs, for those P3HT chromophores in contact with the QDs with a rate constant in the order of 1 to 2×10^{13} s^{-1}, *i.e.* with nearly 100% efficiency. Hence, to increase the overall efficiency of the charge generation the clustering of the QDs should be decreased leading to a smaller average distance of the P3HT chromophore to the nearest QD.

As direct excitation in the first excitonic band led to a similar IQE, in the blend films of P3HT and PbS-BDT QDs and in neat films of PbS-BDT QDs, the charge generation upon direct excitation of the QDs is rather due to direct exciton

dissociation in the QDs rather than (in case of the blend films) photo-induced hole injection in P3HT. This is probably due to the small energy offset between the VB of the QDs and the HOMO of P3HT.[11]

The P3HT:PbS-BDT 90% blend devices can give average efficiency up to 1.8% after optimization. However, despite the evidence of efficient electron transfer from P3HT to PbS QDs, the photovoltaic device with neat PbS-BDT films still shows a higher average PCE (~2.1%) than the devices using the P3HT:PbS blend films. The analysis of the current voltage plots and the comparison of the IQE and its wavelength dependence between photovoltaic devices with a blend P3HT:PbS-BDT QD layer and those with only a neat PbS-BDT QD layer indicate that in the former device the efficiency of the generation of holes and electrons is larger in the wavelength range where P3HT absorbs. Hence, the superior PCE of the latter device could be attributed mainly to a better device absorbance in the near-IR, decreased recombination losses and a better charge carrier transport.

Even at wavelengths where mainly P3HT is excited, the EQE of the blend device only amounted to 50%. This is due to a combination of incomplete absorption of the incident light (considering the difference between the IQE and the EQE), less than 100% efficiency of the charge generation (considering the slow decaying component of more than 350 ps observed by TCSPC) and carrier recombination as suggested by the relatively small fill factor of only 40% (Table III). It means that further improvement of the PCE of the PVs requires to maintain a balance between a more homogeneous distribution of the QDs and sufficient interaction between neighboring QDs to allow percolation and effective electron transport[43].

ACKNOWLEDGEMENTS

This work was supported by the IMEC Leuven (PhD grant to Y.F.) and by the EU through FP7 People Herodot (grant 214954). We are indebted to the research council of KULeuven through GOA 2006/2, 2011/3 and to Belspo through IAP VI/27 en IAP VII/05. Furthermore, funding by the "EWE Nachwuchsgruppe Dünnschichtphotovoltaik" by the EWE AG, Oldenburg, is gratefully acknowledged. Rany Miranti is grateful for a scholarship by the German Academic Exchange Service (DAAD).

[1] W.U. Huynh, J.J. Dittmer, and A.P. Alivisatos, Science **295**, 2425 (2002).

[2] I. Gur, N.A. Fromer, M.L. Geier, and A.P. Alivisatos, Science **310**, 462 (2005).

[3] Y. Kim, S. Cook, S.M. Tuladhar, S.A. Choulis, J. Nelson, J.R. Durrant, D.D.C. Bradley, M. Giles, I. McCulloch, C.-S. Ha, and M. Ree, Nat. Mater. **5**, 197 (2006).

[4] C.J. Brabec, N.S. Sariciftci, and J.C. Hummelen, Adv. Funct. Mater. **11**, 15 (2001).

[5] C.-H.M. Chuang, P.R. Brown, V. Bulović, and M.G. Bawendi, Nat. Mater. **13**, 1 (2014).

[6] D. Zhitomirsky, O. Voznyy, L. Levina, S. Hoogland, K.W. Kemp, A.H. Ip, S.M. Thon, and E.H. Sargent, Nat. Commun. **5**, 1 (2014).

[7] M.A. Green, K. Emery, Y. Hishikawa, W. Warta, and E.D. Dunlop, Prog. Photovolt. Res. Appl. **22**, 1 (2014).

[8] K.M. Noone, E. Strein, N.C. Anderson, P.-T. Wu, S.A. Jenekhe, and D.S. Ginger, Nano Lett. **10**, 2635 (2010).

[9] C. Piliego, H. von Seggern, M. Manca, R. Kroon, M. Yarema, K. Szendrei, M.R. Andersson, and M.A. Loi, J. Mater. Chem. **22**, 24411 (2012).

[10] J. Seo, M.J. Cho, D. Lee, a N. Cartwright, and P.N. Prasad, Adv. Mater. **23**, 3984 (2011).

[11] Y. Firdaus, E. Vandenplas, Y. Justo, R. Gehlhaar, D. Cheyns, Z. Hens, and M. Van der Auweraer, J. Appl. Phys. **116**, 094305 (2014).

[12] O.E. Simonin, J.M. Luther, S. Choi, H.-Y. Chen, J. Gao, A.J. Nozik, and M.C. Beard, Science 334, 1530 (2011).

[13] J. Seo, S.J. Kim, W.J. Kim, R. Singh, M. Samoc, A.N. Cartwright, and P.N. Prasad, Nanotechnology **20**, 095202 (2009).

[14] Z. Tan, T. Zhu, M. Thein, S. Gao, A. Cheng, F. Zhang, C. Zhang, H. Su, J. Wang, R. Henderson, J. Hahm, Y. Yang, and J. Xu, Appl. Phys. Lett. **95**, 063510 (2009).

[15] A.A.R. Watt, D. Blake, J.H. Warner, E.A. Thomsen, E.L. Tavenner, H. Rubinsztein-Dunlop, and P. Meredith, J. Phys. D. Appl. Phys. **38**, 2006 (2005).

[16] Z. Wang, S. Qu, X. Zeng, C. Zhang, M. Shi, F. Tan, Z. Wang, J. Liu, Y. Hou, F. Teng, and Z. Feng, Polymer (Guildf). **49**, 4647 (2008).

[17] K.M. Noone, N.C. Anderson, N.E. Horwitz, A.M. Munro, A.P. Kulkarni, and D.S. Ginger, ACS Nano **3**, 1345 (2009).

[18] M. Nam, J. Park, S.-W. Kim, and K. Lee, J. Mater. Chem. A **2**, 3978 (2014).

[19] J. Yuan, A. Gallagher, Z. Liu, Y. Sun, and W. Ma, J. Mater. Chem. A **3**, 2572 (2015).

[20] Z. Liu, Y. Sun, J. Yuan, H. Wei, X. Huang, L. Han, W. Wang, H. Wang, and W. Ma, Adv. Mater. **25**, 5772 (2013).

[21] E. Strein, A. Colbert, S. Subramaniyan, H. Nagaoka, C.W. Schlenker, E. Janke, S.A. Jenekhe, and D.S. Ginger, Energy Environ. Sci. **6**, 769 (2013).

[22] A.E. Colbert, E.M. Janke, S.T. Hsieh, S. Subramaniyan, C.W. Schlenker, S.A. Jenekhe, and D.S. Ginger, J. Phys. Chem. Lett. **4**, 280 (2013).

[23] G. Chen, J. Seo, C. Yang, and P.N. Prasad, Chem. Soc. Rev. **42**, 8304 (2013).

[24] L.M. Nikolenko and V.F. Razumov, Russ. Chem. Rev. **82**, 429 (2013).

[25] J. Tang and E.H. Sargent, Adv. Mater. **23**, 12 (2011).

[26] C. Piliego, L. Protesescu, S.Z. Bisri, M. V. Kovalenko, and M.A. Loi, Energy Environ. Sci. **6**, 3054 (2013).

[27] H. Choi, J. Kwan Kim, J. Hoon Saong, Y. Kim, and S. Jeong, Appl. Phys. Lett. **102**, 193902 (2013).

[28] J.M. Luther, M. Law, M.C. Beard, Q. Song, M.O. Reese, R.J. Ellingson, and A.J. Nozik, Nano Lett. **8**, 3488 (2008).

[29] See supplementary material at link here for calculation of the weight percentage of P3HT:PbS blend, fluorescence spectra fluorescence decays, calculation of change of transmission of singlet and triplet states, schematic illustration of polaron energy levels, TEM images of

PbS-OLA and PbS-OAm, PIA spectra of a P3HT:PCBM blend film and solar cell performance and dark current density [Supplementary Material].

[30] M. Maus, E. Rousseau, M. Cotlet, G. Schweitzer, J. Hofkens, M. Van der Auweraer, F.C. De Schryver, and A. Krueger, Rev. Sci. Instrum. **72**, 36 (2001).

[31] N. Boens, W. Qin, N. Basaric, J. Hofkens, M. Ameloot, U. Hasselt, D. Building, J. Pouget, J. Lefe, B. Valeur, C. Cedex, E. Gratton, N.D. Silva, I.I. Building, Y. Engelborghs, K. Willaert, A. Sillen, A.J.W.G. Visser, A. Van Hoek, J.R. Lakowicz, H. Malak, I. Gryczynski, A.G. Szabo, and D.T. Krajcarski, Anal. Chem. **79**, 2137 (2007).

[32] Program Developed in a Cooperation between the Management of Technology Institute (Belarusian State University) and The Division of Photochemistry and Spectroscopy (University of Leuven).

[33] E. Fron, M. Van der Auweraer, J. Hofkens, and P. Dedecker, J. Phys. Chem. B **117**, 16422 (2013).

[34] M. Pientka, V. Dyakonov, D. Meissner, a Rogach, D. Talapin, H. Weller, L. Lutsen, and D. Vanderzande, Nanotechnology **15**, 163 (2004).

[35] M.D. Heinemann, K. von Maydell, F. Zutz, J. Kolny-Olesiak, H. Borchert, I. Riedel, and J. Parisi, Adv. Funct. Mater. **19**, 3788 (2009).

[36] M. Law, M.C. Beard, S. Choi, J.M. Luther, M.C. Hanna, and A.J. Nozik, Nano Lett. **8**, 3904 (2008).

[37] I. Moreels, K. Lambert, D. Smeets, D. De Muynck, T. Nollet, J.C. Martins, F. Vanhaecke, A. Vantomme, C. Delerue, G. Allan, and Z. Hens, ACS Nano **3**, 3023 (2009).

[38] Y. Firdaus, S. Kudret, A. Khetubol, W. Maes, L. Lutsen, B. Li, W. Frederickx, S. Flamée, W. Vanderlinden, Z. Hens, S. De Feyter, D. Vanderzande, and M. Van der Auweraer, to be submitted (2015).

[39] P. J. Brown, D. S. Thomas, A. Kohler, J. S. Wilson, J. S. Kim, C. M. Ramsdale, H. Sirringhaus, and R. H. Friend, Phys. Rev. B **67**, 064203 (2003).

[40] F. C. Spano, Chem. Phys. **325**, 22 (2006).

[41] F. C. Spano, J. Chem. Phys. **122**, 234701 (2005)

[42] W. D. Oosterbaan, J. C. Bolsee, A. Gadisa, V. Vrindts, S. Bertho, J. D'Haen, T. J. Cleij, L. Lutsen, C. R. McNeill, L. Thomsen, J. V Manca, and D. Vanderzande, Adv. Funct. Mater. **20**, 792 (2010).

[43] Y. Firdaus, E. Vandenplas, A. Khetubol, D. Cheyns, R. Gehlhaar, and M. Van der Auweraer, J. Appl. Phys., **117**, 095503 (2015).

[44] F. C. Spano, J. Clark, C. Silva, R. H. Friend, J. Chem. Phys. **130**, 074904 (2009).

[45] N. Banerji, S. Cowan, E. Vauthey , and A.J. heeger, J. Phys. Chem. C **115**, 9276 (2011)

[46] I.G. Scheblykin, A. Yartsev, T. Pullerits, V. Gulbinas, and V. Sundström, J. Phys. Chem. B **111**, 6303 (2007).

[47] I.B. Martini, A.D. Smith, and B.J. Schwartz, Phys. Rev. B **69**, 35204 (2004).

[48] T.-Q. Nguyen, I.B. Martini, J. Liu, and B.J. Schwartz, J. Phys. Chem. B **104**, 237 (2000).

[49] S. Cook, H. Liyuan, A. Furube, and R. Katoh, J. Phys. Chem. C **114**, 10962 (2010).

[50] D. Sahoo, K. Sugiyasu, Y. Tian, M. Takeuchi, and I.G. Scheblykin, Chem.Mater. **26**, 4867 (2014).

[51] Y. Xie, Y. Li, L. Xiao, Q. Qiao, R. Dhakal, Z. Zhang, Q. Gong, D. Galipeau, and X. Yan, J. Phys. Chem. C **114**, 14590 (2010).

[52] T. Kobayashi, M. Yoshizawa, U. Stamm, M. Taiji, and M. Hasegawa, J. Opt. Soc. Am. B **7**, 1558 (1990).

[53] S. Trotzky, T. Hoyer, W. Tuszynski, C. Lienau, and J. Parisi, J. Phys. D. Appl. Phys. **42**, 055105 (2009).

[54] S. Westenhoff, W.J.D. Beenken, R.H. Friend, N.C. Greenham, A. Yartsev, and V. Sundström, Phys. Rev. Lett. **97**, 1 (2006).

[55] T. Nakamura, Y. Araki, O. Ito, K. Takimiya, and T. Otsubo, J. Phys. Chem. A **112**, 1125 (2008).

[56] S. Tretiak, a Saxena, R.L. Martin, and a R. Bishop, Phys. Rev. Lett. **89**, 097402 (2002).

[57] O.G. Reid, R.D. Pensack, Y. Song, G.D. Scholes, and G. Rumbles, Chem. Mater. **26**, 561 (2014).

[58] S. Westenhoff, C. Daniel, R.H. Friend, C. Silva, V. Sundström, and A. Yartsev, J. Chem. Phys. **122**, (2005).

[59] D. Sahoo, Y. Tian, G. Sforazzini, L. Anderson, and I.G. Scheblykin, J. Mater. Chem. C **2**, 6601 (2014).

[60] F. Steiner, J. Vogelsang, J.M. lupton, Phys. Rev. Lett. **112**, 137402 (2014)

[61] S. Cook, A. Furube, and R. Katoh, Energy Environ. Sci. **1**, 294 (2008).

[62] J. Guo, H. Ohkita, H. Benten, and S. Ito, J. Am. Chem. Soc. **131**, 16869 (2009).

[63] R. Österbacka, C. An, X. Jiang, and Z. Vardeny, Science. **287**, 839 (2000).

[64] R. Österbacka, C. An, X. Jiang, and Z. Vardeny, Synth. Met. **116**, 317 (2001).

[65] M. Van der Auweraer, P. Ballet, F.C. De Schryver, and A. Kowalczyk, Chem. Phys. **187**, 399 (1994).

[66] F.Fu, X. Ma, C.R. Haughn, J. Benavides, M.F. Doty, S.G. Cloutier, ACS Nano **5**, 9950 (2011).

[67] F. Xu, L.F. Gerlein, R. Haughn, M.F. Doty, S.G. Cloutier, Materials **8**, 1858 (2015).

[68] J. Gao and J.C. Johnson, ACS Nano **6**, 3292 (2012).

[69] T. Förster, *Fluoreszenz Organischer Verbindungen* (Vandenhoeck & Ruprecht, Göttingen, 1951).

[70] T. Főrster, Discuss. Faraday Soc. **27**, 7 (1959).

[71] V.M. Agranovich and M.D. Galanin, *Electronic Excitation Energy Transfer in Condensed Matter* (North Holland Publishing Company, Amsterdam, 1982).

[72] R.J.D. Miller, G.L. McLendon, A.J. Nozik, W. Schmickler, and F. Willig, *Surface Electron Transfer Processes* (VCH New York, 1995).

[73] P.F. Barbara, T.J. Meyer, and M.A. Ratner, J. Phys. Chem. **100**, 13148 (1996).

[74] N.S. Hush, Coord. Chem. Rev., **64**, 135 (1985).

[75] F.C. De Schryver, M. Van der Auweraer, B. Verschuere, and F. Willig in "Separation and Energy migration in Supramolecular Species" NATO ASI Series C, Vol. 214 "Supramolecular Photochemistry" Ed. V. Balzani, D. Reidel Publishing Company, pp 385-403 (1987).

[76] M. Van der Auweraer, G. Biesmans, B. Verschuere, F.C. De Schryver, and F. Willig, Langmuir **3**, 992 (1987).

[77] I. Hwang, D. Moses, and A.J. Heeger, J. Phys. Chem. C **112**, 4350 (2008).

[76] W.J.E. Beek, M.M. Wienk, and R.A.J. Janssen, Adv. Funct. Mater. **16**, 1112 (2006).

[78] H.A. Mizes and E.M. Conwell, Phys. Rev. B **50**, 11243 (1994).

[80] N. Müller, G. Papier, K.-P. Charlé, and F. Willig, Ber. Bunsenges. Phys. Chem **83**, 130 (1979).

[81] G. Papier, K.-P. Charlé, and F. Willig, Ber. Bunsenges. Phys. Chem **86**, 670 (1982).

[82] K. Schulten, H. Staerk, A. Weller, H.-J. Werner, and B. Nickel, Z. Phys. Chem **101**, 371 (1976).

[83] H. Sirringhaus, P.J. Brown, R.H. Friend, M.M. Nielsen, K. Bechgaard, and A.J.H. Spiering, Nature **401**, 685 (1999).

[84] J.A.E.H. van Haare, E.E. Havinga, J.L.J. van Dongen, R.A.J. Janssen, J. Cornil, and J-.L. Brédas, Chem. - Eur. J. **4**, 1509 (1998).

[85] J.A. Blackman and M.K. Sabra, Phys. Rev. B **47**, 15437 (1993).

[86] C. Silva, A. Dhoot, D. Russell, M. Stevens, A. Arias, J. MacKenzie, N. Greenham, R. Friend, S. Setayesh, and K. Müllen, Phys. Rev. B **64**, 125211 (2001).

[87] S.D. Dimitrov and J.R. Durrant, Chem. Mater. **26**, 616 (2014).

[86] C. Deibel, D. Mack, J. Gorenflot, A. Schöll, S. Krause, F. Reinert, D. Rauh, and V. Dyakonov, Phys. Rev. B **81**, 085202 (2010).

[88] J. Zhang and X. Jiang, J. Phys. Chem. B **112**, 9557 (2008).

[90] Y. Firdaus, A. Khetubol, S. Kudret, H. Dilien, W. Maes, L. Lutsen, D. Vanderzande, and M. Van der Auweraer, Photonics Sol. Energy Syst. Iv **8438**, 84381G (2012).

[91] P. Reiss, E. Couderc, J. De Girolamo, and A. Pron, Nanoscale **3**, 446 (2011).

[92] L. Pandey, and M. Van der Auweraer, J. Appl. Phys. **110**, 053712 (2010)

Supporting information

Charge separation dynamics at bulk heterojunctions between poly(3-hexylthiophene) and PbS quantum dots

Yuliar Firdaus,[1] Rany Miranti,[2] Eduard Fron,[1] Adis Khetubol,[1] Erwin Vandenplas,[3] David Cheyns,[3] Holger Borchert,[2] Jürgen Parisi,[2] Mark Van der Auweraer [1,a)]

[1] *Laboratory of Photochemistry and Spectroscopy, Division of Molecular Imaging and Photonics, Chemistry Department, KULeuven, Celestijnenlaan 200F, B2404, 3001 Leuven, Belgium*

[2] *University of Oldenburg, Department of Physics, Energy and Semiconductor Research Laboratory, Carl-von-Ossietzky-Str. 9-11, 26129 Oldenburg, Germany*

[3] *Imec vzw, Kapeldreef 75, 3001 Leuven, Belgium*

[a)] Author to whom correspondence should be addressed. Electronic mail: mark.vanderauweraer@chem.kuleuven.be.

Supporting Information 1: Weight percent of the different components in P3HT:PbS blends

Assuming that the PbS QDs are not capped by ligands the weight percent of PbS QDs in the P3HT:PbS blends amounts to:

$$\text{wt\%} = 100\% \times \frac{w_{PbS}}{w_{PbS} + w_{P3HT}},$$

w_{P3HT} is the weight of P3HT (in gram) added to the casting solution and w_{PbS} is the weight of PbS (in gram). w_{PbS} can be determined unambiguously from the volume of PbS solution ($V_{PbS,solution}$) (in l) added to the casting solution, the concentration of QDs (c_{PbS}) (in mol/l) and the diameter of the PbS core of the QDs (the concentration being *e.g.* ~690 µM for the solution of PbS QDs with a diameter of 2.4 nm obtained from Evident Technology). For this solution the volume of a single QD (V_{1PbS}) amounts to 7.235×10^{-21} cm^3.

This yields for w_{PbS}

$$w_{PbS} = N_{PbS} V_{1PbS} D_{PbS} = N_A c_{PbS} V_{PbS,solution} V_{1PbS} D_{PbS},$$

where D_{PbS} is the density of PbS (7.61 g/cm^3) and N_A is the Avogadro constant.

If the ligands are considered, the weight percent of PbS QDs in P3HT:PbS blends becomes:

$$\text{wt\%} = 100\% \times \frac{w_{PbS}}{w_{PbS} + w_{P3HT} + w_{ligand}}$$

with $w_{ligand} = M_{ligand} \times n_{ligand} = 80 M_{ligand} \times \frac{N_{PbS}}{N_A} = M_{ligand} \times \frac{80 \times w_{PbS}}{N_A V_{1PbS} D_{PbS}} = M_{ligand} \times 80 \times c_{PbS} V_{PbS,solution}$

w_{ligand} is the weight of the ligands (in gram) added to the casting solution, M_{ligand} is the molar mass of the ligands (g/mol), N_{PbS} is the number of PbS QDs which can be calculated from the known concentration of colloidal QDs (c_{PbS}) and the volume of PbS QD solution ($V_{PbS,solution}$) added to the casting solution. N_{ligand} is calculated knowing that each QD is capped by ~80 ligands, hence (N_{ligand}=80N_{PbS}). This ratio was estimated from the NMR-spectrum of a solution of PbS QDs capped by OLA using using CH_2Br_2 as a concentration standard[1]. We also assumed that the ligand exchange replaced all the initial ligands of OLA which is a good estimate for BDT or OT.

Throughout the manuscript we used the weight % assuming no ligands (first column in Table S1) as operational parameter as this could be determined completely unambiguously and without making any assumptions on e.g. the number of ligands per quantum dot (QD). Knowing the number of ligands per quantum dot and the density of P3HT (1.17 g/cm³), of PbS (7.61 g/cm³) and of the ligands it is then also simple to calculate the volume % occupied by P3HT, the PbS QD and the ligands using the relation.

$$v_i = \frac{\frac{w_i}{\rho_i}}{\sum \frac{w_i}{\rho_i}}$$

Where v_i an w_i are the weight and volume fractions of compound i and ρ_i is the density of compound i (0.895 g/ml for OLA, 1.24 g/ml for BDT, 0.782 g/ml for OAm and 0.843 g/ml for OT)

TABLE S1. Weight% and volume % of PbS QDs and vol % of the ligand in P3HT:PbS blends taking into account the ligand shells.

wt% PbS (assuming no ligand)	wt% PbS (OLA ligand)	wt% PbS (OAm ligand)	wt% PbS (OT ligand)	wt% PbS (BDT ligand)
60	43	51	50	50
75	50	61	59	60
90	56	70	68	69
100	60	76	74	75
wt% PbS (assuming no ligand)	vol % PbS (OLA ligand)	vol% PbS (OAm ligand)	vol% PbS (OT ligand)	vol% PbS (BDT ligand)
60	8.9	11.9	11.6	13.3
75	11.1	16.0	15.7	18.8
90	13.3	21.0	20.3	26.1
100	14.7	24.8	23.9	32.2
wt% PbS (assuming no ligand)	vol % ligand (OLA ligand)	vol% ligand (OAm ligand)	vol% ligand (OT ligand)	vol% ligand (BDT ligand)
60	51.7	35.9	37.0	28.0
75	64.3	48.6	49.8	39.6
90	76.9	63.6	64.7	54.8
100	85.3	75.2	76.1	67.8

Supporting Information 2: Fluorescence spectra

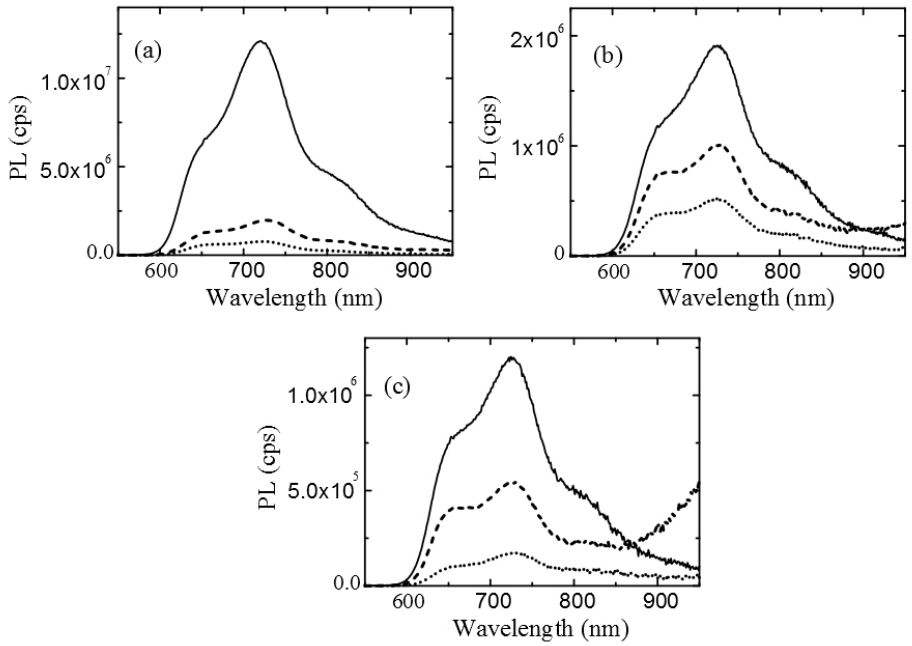

Figure S1. Photoluminescence (PL) spectra of the P3HT:PbS film cast from chloroform ((a) 60%, (b) 75%, (c) 90% QDs)). The QDs were capped with OLA ligands (dashed lines) and BDT ligands (dotted lines). Solid lines: PL spectra of neat P3HT films prepared from a casting solution containing the same amount of P3HT as in respective blend solutions before spin-casting ((a) 8.5 mg/ml, (b) 5.4 mg/ml, (c) 3.8 mg/ml). Excitation occurred at 488 nm and the spectra were not corrected for the difference in P3HT absorbance at the excitation wavelength.

Supporting Information 3: Fluorescence decays

TABLE S2. Decay times (τ_i) and amplitudes (P_i) of the fluorescence of a neat P3HT film at different detection wavelengths determined by TCSPC (and at different intensity for λ_{em}=750 nm). The fluorescence decay fitted to bi-exponential function with the exception for λ_{em}=750 nm, which analyzed as a single exponential.

λ_{em} (nm)	Laser energy $\times 10^9$ (photons/(pulse.cm²))	$\frac{A_1}{\sum_i A_i}$ (%)	P_1(%)	τ_1 (ps)	$\frac{A_2}{\sum_i A_i}$ (%)	P_2(%)	τ_2 (ps)	χ^2
650	2.8	0.41	4.7	47	0.59	95.3	671	1.07
675	2.8	0.35	3.3	40	0.65	96.7	647	1.02
700	2.8	0.40	3.6	36	0.60	96.4	667	1.06
725	2.8	0.27	2	38	0.73	98	680	1.063
750	0.83	-	-	-	1.0	100	793	1.1
	2.8	-	-	-	1.0	100	761	1.09
	4.6	-	-	-	1.0	100	758	1.09
	5.8	-	-	-	1.0	100	760	1.08
	7.9	-	-	-	1.0	100	730	1.16

TABLE S3. Fluorescence decay times (τ_i) and amplitudes (P_i) of pristine P3HT films and blend P3HT:PbS-BDT films obtained from the TRFA global analysis program, $<\tau>$ is the average fluorescence decay time.

Samples	detection (nm)	$\frac{A_1}{\sum_i A_i}$ (%)	τ_1 (ps)	$\frac{A_2}{\sum_i A_i}$ (%)	τ_2 (ps)	$<\tau>$ (ps)	% of average PL decay time reduction	χ^2
P3HT	650	0.41	46.9	0.59	671	415	-	1.07
	725	0.27	37.6	0.73	680	505	-	1.06
+PbS-OLA 60%	650	0.38	89	0.62	670	452	-	1.03
	725	0.32	108	0.68	671	490	-	1.02
+PbS-OLA 75%	650	0.44	81	0.56	657	406	-	1.09
	725	0.45	99	0.55	648	401	-	1.02
+PbS-OLA 90%	650	0.43	98	0.57	703	441	-	1.08
	725	0.36	115	0.64	700	491	-	1.03
+PbS-OAm 60%	650	0.60	55.3	0.40	302	154	63	1.13
	725	0.52	53.2	0.48	307	174	66	0.99
+PbS-OT 60%	650	0.39	96.2	0.61	552	372	10	1.12
	725	30	126	0.69	555	424	16	1.13

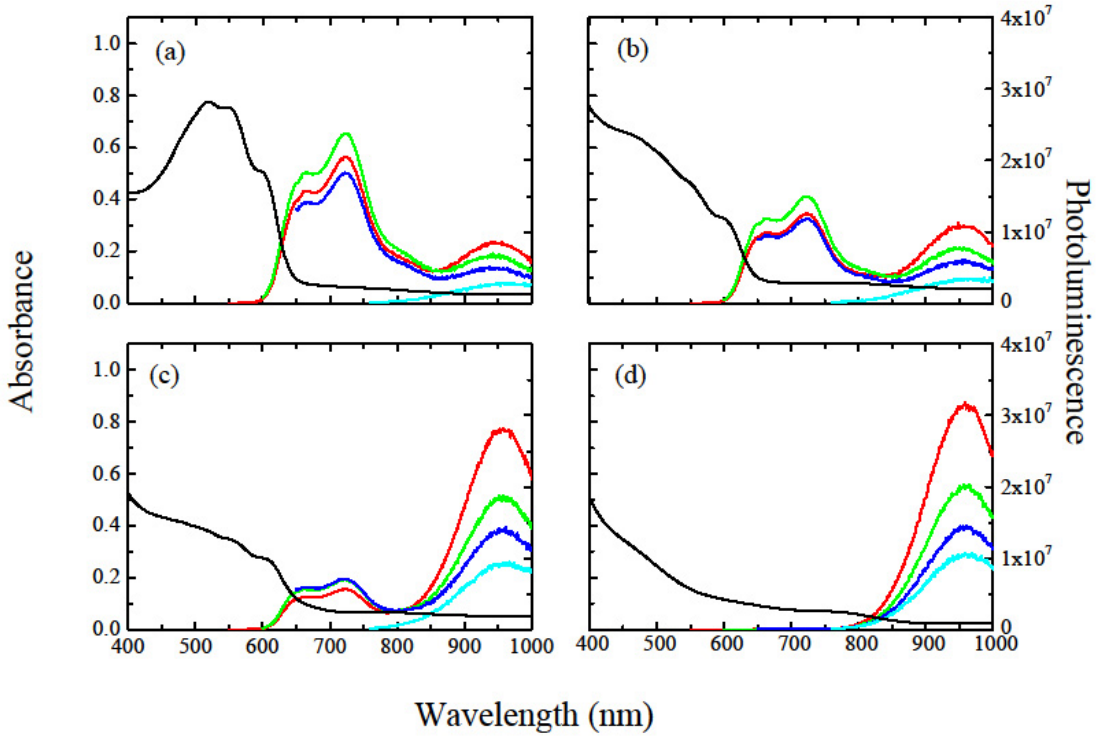

Figure S2. Absorption and PL spectra of films of P3HT:PbS-OLA blends with a loading of 60% (a), 75% (b) and 90% (c) PbS-OLA QDs and of film of neat PbS-OLA QDs film (d). The PL spectra are shown for different excitation wavelengths (λ_{exc}=488 nm (red), 550 nm (green), 600 nm (blue), 730 nm (cyan)). The PL from 600-850 nm is related to P3HT and the Pl from 750-1000 nm is related to the PbS QDs-OLA.

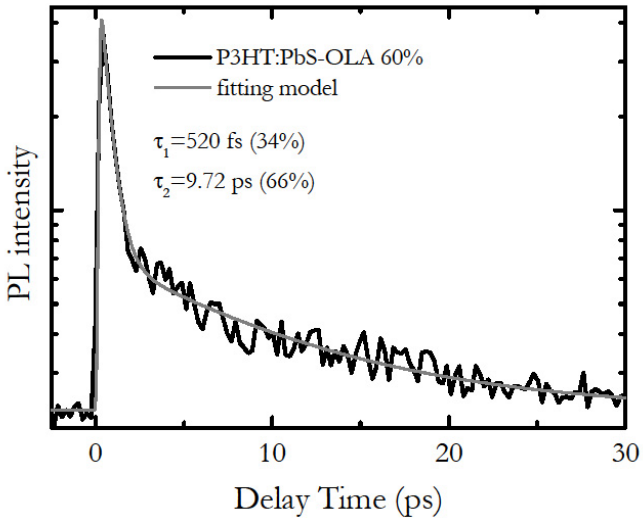

Figure S3. Fluorescence decays determined by fluorescence up-conversion of P3HT:PbS-OLA 60% (black line) films with emission of 650 nm (~1.9 eV). Also shown fitting to bi-exponential model (red line).

Supporting Information 4: Estimation of the change of transmission for singlet and triplet excitons in P3HT in PIA experiments

The ratio $\frac{\Delta T}{T}$ is proportional to the absorbance change:

$$\frac{\Delta T}{T} = \ln(10) \times \Delta A = \ln(10) \times C\varepsilon d$$

where d is thickness of sample (in cm) and ε is the molar extinction coefficient (in $M^{-1}cm^{-1}$), which is estimated to be 50 000 $M^{-1}cm^{-1}$. The thickness of the sample is 100 nm or 10^{-5} cm. C is the pseudostationary concentration of singlet or triplet states (in mol/L) and can be written as $C = \eta c_{abs} \times \tau$, with η being the efficiency of singlet or triplet formation, c_{abs} the generation rate of excited species corresponding to the concentration of photons absorbed per second (in mol/(s·l)) and τ being the estimated singlet or triplet decay time (in s). In this approach we assume that the modulation frequency of the laser is much smaller than the inverse decay time of the excited species.

The generation rate of excited states c_{abs} can be calculated as $c_{abs} = \frac{n_{photon}(1-10^{-A})}{N_A V}$, where N_A is Avogadro's number, V is volume of the film illuminated by the laser absorption (~4×10^{-8} liter in our experiments) and A is sample absorption. The number of incident photons per second, n_{photon} , is estimated to equal *ca.* 4×10^{16} photons/s for a 15 mW laser at 532 nm and c_{ab} was determined to be 1.06 M/s for an absorption of the sample of 0.434.

The decay times of singlet and triplet excitons used in the calculation are 1 ns and 1 ms, respectively. Assuming 100% in efficiency of the singlet or triplet exciton formation, the estimated values of $\frac{\Delta T}{T}$ are found to be *ca.* 1.2×10^{-9} and 1.2×10^{-3} for a singlet and triplet states, respectively. Or if the efficiency of the formation of singlet or triplet excitons is 10% the estimated values of $\frac{\Delta T}{T}$ are 1.2×10^{-10} and 1.2×10^{-4} respectively. For the molar extinction coefficient, ε, a value of $5x10^4$ $M^{-1}cm^{-1}$ was assumed. If the real values of ε are smaller this will yield smaller values of $\frac{\Delta T}{T}$.

Supporting Information 5: Polaron energy levels

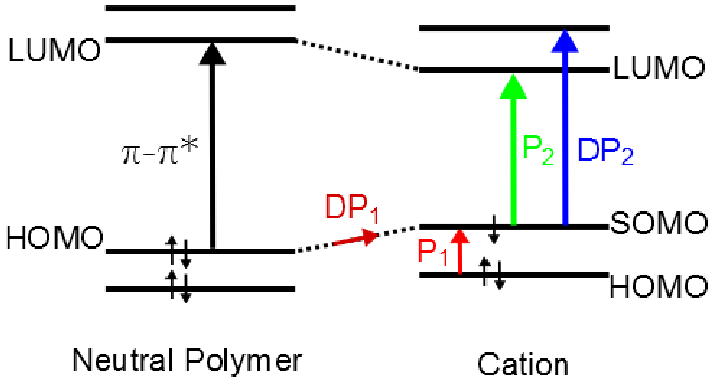

Figure S4. Simple picture of energy levels and electronic transitions of neutral polymer, localized and delocalized polaron interpreted in analogy to spectra of radical cations of oligothiophenes[2–4].

Supporting Information 6: PIA spectra of P3HT:PCBM 50 wt%

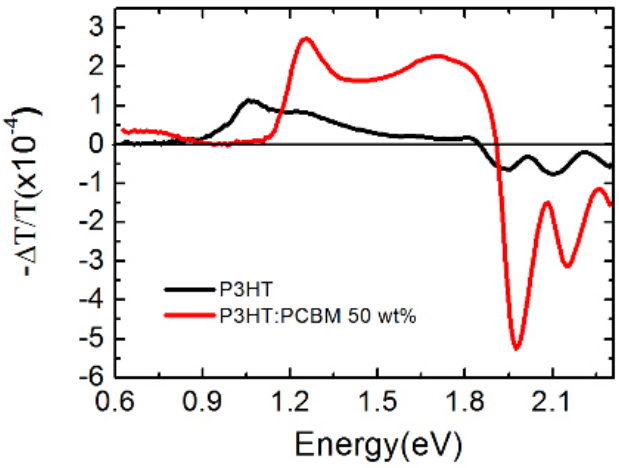

Figure S5. PIA spectrum of pristine P3HT (black) and P3HT:PCBM 50 wt% (red) blend films.

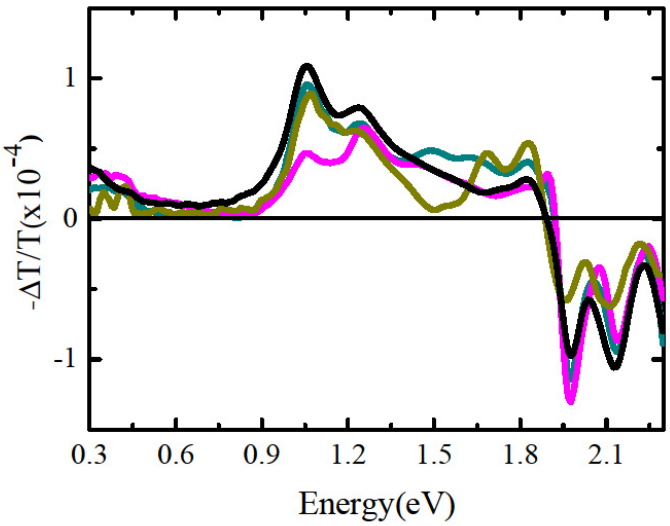

Figure S6. PIA spectrum of pristine P3HT (black) and P3HT:PbS 60% films with different PbS capping ligands: OLA(dark yellow), OAm (dark cyan), OT (magenta);

Supporting Information 7: Structural change of PbS-OAm QDs compared to PbS-OLA QDs

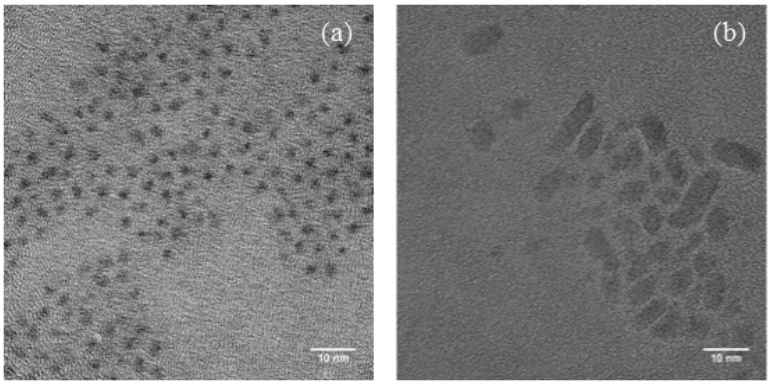

Figure S7. High resolution TEM image of PbS QDs with (a) OLA ligands and (b) after ligand exchange to OAm.

Supporting Information 8: Dark current density in photovoltaic devices with PbS QDs

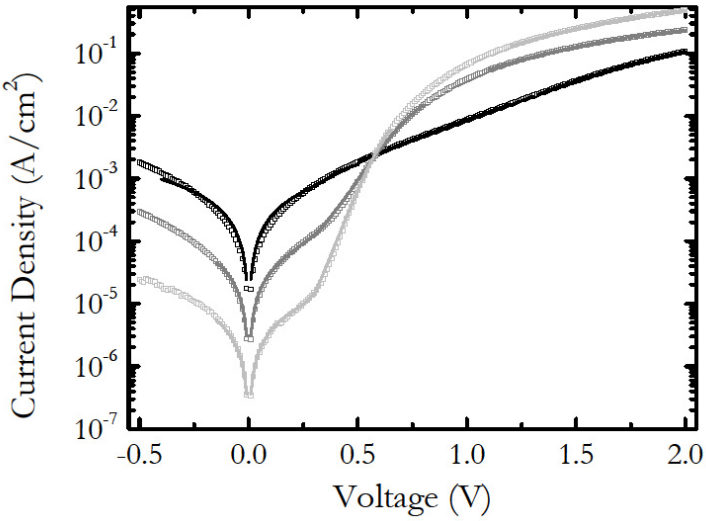

Figure S8. Current density-Voltage (*J-V*) characteristics in the dark for the P3HT:PbS-BDT and neat PbS-BDT photovoltaic devices. The open symbols are the experimentally measured data, while the solid lines are fits according to an equivalent circuit model including series and shunt resistance[5] □, ___: ITO/PEDOT:PSS/P3HT:PbS-BDT 90%/Ca/Ag, □, ___ : ITO/PEDOT:PSS/P3HT:PbS-BDT 90%/PbS-BDT(5 mg/ml)/Ca/Ag, □, ___: ITO/PEDOT:PSS/ PbS-BDT/PbS-BDT(5 mg/ml)/Ca/Ag.

TABLE S4. Diode parameters obtained from the current density-voltage characteristics in the dark (dark current density fitted with equivalent circuit model) of the P3HT:PbS-BDT 90% and neat PbS-BDT photovoltaic devices build up in the following way: (ITO/PEDOT:PSS/active layer/PbS-BDT (5 mg/ml)/Ca/Ag). R_S, R_{SH}, A, J_0 and n are, respectively, the series resistance, the shunt resistance, the device area, the dark saturation current density and the ideality factor. The parameters of each sample were averaged from dark *J-V* characteristics fitting of 3 different cells.

Samples	$R_S \cdot A$ ($\Omega \cdot cm^2$)	$R_{SH} \cdot A$ ($\Omega \cdot cm^2$)	J_0 (A/cm^2)	n
P3HT:PbS-BDT 90% [a]	22±8	$(4.6\pm1.7)\times10^3$	$(2.1\pm1.2)\times10^{-4}$	9.8±1.8
P3HT:PbS-BDT 90%	31±6	$(2.6\pm0.4)\times10^4$	$(1.7\pm0.8)\times10^{-6}$	3.1±0.2
PbS-BDT	20±13	$(3\pm1.3)\times10^5$	$(2.8\pm0.4)\times10^{-8}$	1.9±0.1

[a] Structure of the photovoltaic devices: ITO/PEDOT:PSS/active layer/Ca/Ag, i.e., without an additional PbS layer deposited on top of the active layer.

References

[1] I. Moreels, B. Fritzinger, J.C. Martins, and Z. Hens, J. Am. Chem. Soc. **130**, 15081 (2008).

[2] J. Guo, H. Ohkita, H. Benten, and S. Ito, J. Am. Chem. Soc. **131**, 16869 (2009).

[3] H. Sirringhaus, P.J. Brown, R.H. Friend, M.M. Nielsen, K. Bechgaard, and A.J.H. Spiering, Nature **401**, 685 (1999).

[4] J.A.E.H. van Haare, E.E. Havinga, J.L.J. van Dongen, R.A.J. Janssen, J. Cornil, and J.-L. Brédas, Chem. - Eur. J. **4**, 1509 (1998).

[5] Y. Firdaus, E. Vandenplas, Y. Justo, R. Gehlhaar, D. Cheyns, Z. Hens, and M. Van der Auweraer, J. Appl. Phys. **116**, 094305 (2014).